Cell geometry, signal dampening, and a bimodal transcriptional response underlie the spatial precision of an ERK-mediated embryonic induction

Géraldine Williaume, Sophie de Buyl, Cathy Sirour, Nicolas Haupaix, Rossana Bettoni, Kaoru Imai, Yutaka Satou, Geneviève Dupont, Clare Hudson, Hitoyoshi Yasuo

Cell geometry, signal dampening, and a bimodal transcriptional response underlie the spatial precision of an ERK-mediated embryonic induction

Géraldine Williaume[1,8], Sophie de Buyl[2,3,8], Cathy Sirour[1,8], Nicolas Haupaix[1,7], Rossana Bettoni[2,3,4], Kaoru S. Imai[5], Yutaka Satou[6], Geneviève Dupont[4*], Clare Hudson[1,8*] and Hitoyoshi Yasuo[1,8,9*]

1- Laboratoire de Biologie du Développement de Villefranche-sur-mer, Institut de la Mer de Villefranche-sur-mer, Sorbonne Université, CNRS, 06230 Villefranche-sur-mer, France.
2- Applied Physics Research Group, Vrije Universiteit Brussel, Pleinlaan 2, B-1050 Brussels, Belgium.
3- Interuniversity Institute of Bioinformatics in Brussels, ULB-VUB, La Plaine Campus, B-1050 Brussels, Belgium.
4- Unité de Chronobiologie Théorique, Faculté des Sciences, CP231, Université Libre de Bruxelles (ULB), Boulevard du Triomphe, B-1050 Brussels, Belgium.
5- Department of Biological Sciences, Graduate School of Science, Osaka University, Toyonaka, Osaka 560-0043, Japan.
6- Department of Zoology, Graduate School of Science, Kyoto University, Sakyo, Kyoto 606-8502, Japan.
7- Current address: Max Planck Institute for Biophysical Chemistry, Am Fassberg 11, 37077 Göttingen, Germany.
8- These authors contributed equally
9- Lead contact
* Corresponding authors: yasuo.hitoyoshi@imev-mer.fr, clare.hudson@imev-mer.fr, Genevieve.Dupont@ulb.be

SUMMARY

Precise control of lineage segregation is critical for the development of multicellular organisms but our quantitative understanding of how variable signaling inputs are integrated to activate lineage-specific gene programs remains limited. Here we show how precisely two out of eight ectoderm cells adopt neural fates in response to ephrin and FGF signals during ascidian neural induction. In each ectoderm cell, FGF signals activate ERK to a level that mirrors its cell contact surface with FGF-expressing mesendoderm cells. This gradual interpretation of FGF inputs is followed by a bimodal transcriptional response of the immediate early gene, *Otx*, resulting in its activation specifically in the neural precursors. At low levels of ERK, *Otx* is repressed by an ETS family transcriptional repressor, ERF2. Ephrin signals are critical to dampen ERK activation levels across ectoderm cells so that only neural precursors exhibit above-threshold levels, evade ERF repression, and "switch on" *Otx* transcription.

INTRODUCTION

The development of a multicellular organism is a reproducible process during which cells adopt different identities with exquisite spatiotemporal precision. However, our quantitative understanding of how cells interpret signals from their environment and activate specific gene programs to attain such precision remains limited. In this study, we address this question focusing on the extracellular signal-regulated kinase (ERK) signaling pathway in the context of an embryonic induction.

ERK is the effector molecule of the evolutionary conserved Ras/ERK cascade that operates downstream of receptor tyrosine kinases (RTKs) (Lemmon and Schlessinger, 2010). Differences in the temporal dynamics, amplitude, or cumulative load of the ERK response can promote distinct cellular responses (Aoki et al., 2013; Blum et al., 2019; Ebisuya et al., 2005; Johnson and Toettcher, 2019; Pokrass et al., 2020; Ryu et al., 2015; Santos et al., 2007; Simon et al., 2020). One of the ways that ERK alters the developmental trajectory of a cell is by modifying the activity of transcription factors and thus the gene expression profile of the responding cell. However, in the context of *in vivo* multicellular systems, quantitative studies addressing how ERK impacts its direct target genes are only beginning to emerge (van Boxtel et al., 2018; Johnson and Toettcher, 2019; Lim et al., 2013, 2015; Pokrass et al., 2020).

Ascidians are marine invertebrate chordates that develop with a fixed cell lineage and small number of cells. Cellular inductions in ascidian embryos are proposed to be largely cell-contact-dependent (Guignard et al., 2020). Early neural induction in ascidian embryos refers to the onset of specification of part of the central nervous system, anterior brain and dorsal neural tube (Hudson, 2016). It takes place during a single cell cycle of approximately 30 minutes at the 32-cell stage of development where FGF9/16/20 in mesendoderm cells, acting as a short-range inducer, directly activates *Otx* in ectoderm via ERK activation (Figure 1A) (Bertrand et al., 2003; Hudson et al., 2003, 2016; Miyazaki et al., 2007). While all eight pairs of ectoderm cells are competent for neural induction and are in direct contact with the underlying mesendoderm cells that express *FGF9/16/20,* only the neural precursors, a6.5 and b6.5, which have the largest area of cell surface contact, exhibit ERK activation and express *Otx* (Figures 1A-C, S1A, and S1B) (Ohta and Satou, 2013; Tassy et al., 2006). The a6.7 cells segregate into neural and epidermal lineages at the next cell division. These cells have the next highest area of cell surface contact with FGF-expressing cells and occasionally

express *Otx* (Ohta and Satou, 2013; Tassy et al., 2006). An ephrin ligand, Efna.d, expressed in the ectoderm cells themselves, acts via Eph3/p120RasGAP to attenuate the Ras-MEK-ERK cascade and prevent ectopic *Otx* activation in non-neural ectoderm cells (Figure 1A) (Haupaix et al., 2013; Ohta and Satou, 2013; Ohta et al., 2015; Picco et al., 2007). Ectoderm cells with the highest cell surface contact with FGF-expressing mesendoderm cells have, inversely, the lowest cell surface contact with ephrin-expressing ectoderm cells (Figure 1B) (Ohta and Satou, 2013; Ohta et al., 2015; Tassy et al., 2006). Interaction of these two antagonistic signaling inputs results in expression of *Otx* in precisely four cells within a field of 16 competent ectoderm cells.

In previous studies, non-quantitative means of detecting ERK activation and *Otx* gene expression were used. Therefore, how antagonistic FGF and ephrin signals lead to neural lineage-specific *Otx* transcriptional activation remained unclear. For example, it was unknown if the ERK activation response to FGF9/16/20 is gradual or switch-like during this binary fate decision. It was also not clear what role ephrin/Eph signals play in establishing the pattern of ERK activation or the exact nature of the transcriptional response of the *Otx* gene. In this study, we addressed these issues, measuring, in a quantitative manner, the activation of both ERK and *Otx* expression, using primarily *Ciona intestinalis*.

RESULTS

FGF-dependent ERK activation levels in ectoderm cells mirror the contact area with FGF-expressing cells

Early neural induction in ascidian embryos is dependent on cell-cell contact with *FGF9/16/20*-expressing mesendoderm cells during the 32-cell stage (Miyazaki et al., 2007; Tassy et al., 2006). We used semi-quantitative single molecule fluorescence *in situ* hybridization (smFISH) for *FGF9/16/20* to quantify the number of smFISH spots in each mesendoderm cell nucleus at the 32-cell stage. Among the A-lineage mesendoderm cells, similar levels of *FGF9/16/20* transcripts were detected, whereas levels were variable among B-line cells (Figure S1A). Since a-line cells are in contact almost exclusively with the A-line mesendoderm cells that express similar levels of inducer, we focused our analysis on the four pairs of a-line cells, namely a6.5, a6.6, a6.7 and a6.8 (Figures 1A, S1A, and S1B). The average area of cell surface contact between each ectoderm cell and A-line mesendoderm

(n=26 per cell type) measured in μm^2 (mean±SD) was 2732.2±248.5 for a6.5, 1668.8±409.0 for a6.7, 762±175.4 for a6.6 and 409±138.1 for a6.8. In order to compensate for small differences in embryo and cell size, for each cell, we normalized the cell surface contact area by dividing it with its total cell surface area, to obtain the relative area of cell surface contact (Figure 1B). Considering each embryo-half independently, in 100% of cases, a6.5 exhibited a higher relative cell surface contact than a6.7 (a6.5>a6.7), with a6.7>a6.6 at 100% and a6.6>a6.8 at 96 %. The relative area of cell surface contact to FGF-expressing mesendoderm cells for each a-line cell correlates strongly and inversely to the relative area of cell surface contact with neighboring ephrin-expressing ectoderm cells, consistent with previous reports (Ohta and Satou, 2013; Tassy et al., 2006) (Figure 1B).

To quantify active ERK levels in individual a-line cells at the late 32-cell stage, we used immunofluorescence (IF) staining for dually phosphorylated ERK (dpERK) together with anti-Histone H3 (H3) to segment nuclei (Figure 1C). Embryos were processed under identical conditions (same tube/coverslip/acquisition session) and the mean pixel intensity of the nuclear dpERK IF signal measured. Considering each half embryo independently, a6.5 exhibited a higher dpERK IF signal level than a6.7 in 99% of cases (a6.5>a6.7), with a6.7>a6.6 at 94% and a6.6>a6.8 at 83% (Figures 1D and S1C). The pattern of nuclear dpERK IF signal between a-line cells appeared remarkably similar to the area of cell surface contact measured between inducing and responding cells (Figures 1B and 1D).

Similar results were obtained with the biosensor ERK-KTR in *Phallusia mammillata* embryos (Figures 1F and S1E). ERK-KTR resides in the nucleus and is exported into the cytoplasm following phosphorylation by ERK. The cytoplasmic/nuclear (C/N) ratio of ERK-KTR signals measured for each a-line cell at the late 32-cell stage (t=6') was comparable to measurements with anti-dpERK IF, although we were unable to detect significant differences between a6.6 and a6.8. The temporal dynamics of ERK activation can exhibit distinct profiles such as sustained, transient or oscillatory (Albeck et al., 2013; de la Cova et al., 2017; Ebisuya et al., 2005; Francavilla et al., 2013; Santos et al., 2007; Shankaran et al., 2009). During the period of analysis, C/N ratios normalized to a6.8 levels (see STAR Methods for details) appeared stable with consistently higher levels of ERK activity in a6.5 compared to a6.6 and a6.7 ($P \leq 0.0006$, in paired t-tests) (Figures 1F and S1G).

The first cell division of ascidian zygotes bisects the embryo into two mirror-image bilateral halves. Inhibition of FGF signaling in only one half of the embryo allowed us to

compare ERK activation levels between control and dnFGFR-injected halves within the same embryo (Figures 2A, S1F, and S1G). While the ratio of injected/control side nuclear dpERK IF signals showed no statistically significant difference from 1 for *PH-GFP* half-injected control embryos, *dnFGFR* half-injected embryos showed a significant reduction in nuclear dpERK IF signals in a6.5, a6.7 and a6.6 (Figure 2A). For ERK-KTR, a significant reduction was seen in a6.5 and a6.7 *dnFGFR* injected sides (Figure S1F). Treatment of embryos with a pharmacological inhibitor of MEK, U0126, showed similar results (Figures S1D and S1H).

The similarity in the pattern of nuclear ERK activation levels in a-line cells and their relative areas of cell surface contact with mesendoderm cells (compare Figures 1B-1D) suggests a causal correlation between them. Indeed, we observed a high degree of correlation (Spearman correlations of 0.69-0.89, $P<0.0001$) between the relative area of cell surface contact with mesendoderm cells and ERK activation levels measured in individual ectoderm cells (Figures 1E and S2A). This is consistent with the level of FGF-signal input being proportional to the area of cell surface contact with FGF-expressing cells. However, there is an inverse relationship between the area of cell surface contact with FGF-expressing mesendoderm cells and that of ephrin-expressing ectoderm cells (Figure 1B). We therefore next addressed the role of ephrin/Eph signals in this process.

ephrin/Eph signals lower the amplitude of ERK activation

To inhibit Eph signals, we used dominant negative forms of Eph3 (*Eph3ΔC*) and p120RasGAP (*RGΔGAP*) and a small molecule inhibitor of EphB4, NVP-BHG712 (henceforth NVP) (Fiuza et al., 2020; Haupaix et al., 2013; Picco et al., 2007). Since cell surface contacts correlate with ERK activation levels in the 32-cell *Ciona* embryo (Figure 1E) and ephrin/Eph signals mediate cell adhesion and cell shape in many developmental contexts (Klein, 2012), we first verified that inhibition of ephrin/Eph signals does not measurably alter cell surface contacts in 32-cell stage *Ciona* embryos. No significant difference in cell surface contacts was detected between control and *Eph3ΔC*-injected cells within the same embryo or between groups of control and NVP-treated embryos (Figures 2B and S2B).

Injecting either *Eph3ΔC* or *RGΔGAP* into one cell of the two-cell stage embryo resulted in an increase in dpERK IF signal on the injected side, with statistical support for all cells (Figure 2A). NVP-treatment similarly results in an increase in ERK activation levels (Figure S2C). Considering each half embryo independently, a6.5>a6.7 was observed in 99%

of cases; with a6.7>a6.6 at 100% and a6.6>a6.8 at 82% in NVP-treated embryos (Figures 2C and S1C). We detected a high degree of correlation (Spearmen correlations ranging from 0.79 to 0.94, P<0.0001) between the relative area of cell surface contact with FGF-expressing cells and ERK activation levels for each a-line ectoderm cell even in the absence of Eph signals (Figures 2D and S2A). We conclude that Eph signals are not critical to establish the differential ERK activation pattern between the different a-line cells, but impacts the amplitude of the ERK response.

Gradual ERK activation response of ectoderm cells to increasing doses of FGF

Dose responses of ERK activation to growth factor stimulation can be switch-like (ultrasensitivity, bistability), gradual or linear (Aoki et al., 2011; Ferrell Jr. and Machleder, 1998; Huang and Ferrell, 1996; MacKeigan et al., 2005; Markevich et al., 2004; Nunns and Goentoro, 2018; Perrett et al., 2013; Santos et al., 2007). Dissected ectodermal explants of ascidian embryos develop into epidermis when left untreated, whereas explants treated with bFGF adopt neural fates (Bertrand et al., 2003; Hudson and Lemaire, 2001; Inazawa et al., 1998). Although we do not know if bFGF binds and activates the FGFR with the same kinetics as the endogenous FGF, this *ex-vivo* experimental setting allowed us to control the concentration of FGF ligand.

We conducted a dose response analysis of 12 experimental replicas of control versus NVP-treated ectodermal explants, treated with different concentrations of bFGF from the very early 32-cell stage for 18 minutes, when dpERK levels become relatively stable (Figures 3A, 3B, and S2D-S2G). Curve fitting with a Hill function to these dose responses gave a best-fit Hill coefficient of 0.77 (confidence interval 0.51 to 1.15; r^2=0.8032, n=115) for control explants and 0.59 (confidence interval 0.29 to 1.11; r^2=0.6627, n=115) for NVP-treated explants. Thus, in this experimental setting, we found that ERK responds gradually to different concentrations of FGF and that Eph signals lower the amplitude but only slightly increase the sensitivity of the ERK response to bFGF.

Measuring nuclear dpERK IF signals in ectodermal explants treated with different concentrations of bFGF allowed us to address the dose response of individual cells and to distinguish nuclear and cytoplasmic ERK activation, which can show different kinetics (Shindo et al., 2016). This single-cell level dose response analysis revealed that ERK activation is variable and gradual, consistent with the *in vivo* ERK response to endogenous

FGF9/16/20 (Figures 3C, S2H, and S2I). Altogether, our *in vivo* and *ex vivo* data provided no evidence for bimodality under any of the conditions tested (Figures S3A, S3B, and S3D) suggesting a gradual ERK response to different levels of FGF signal input.

Mathematical modeling of differential FGF and ephrin signaling inputs

Our data shows a correlation between the area of cell surface contact with FGF-expressing mesendoderm cells and the level of ERK activation in ectoderm cells whether or not the ephrin/Eph signaling pathway is intact (Figures 1E, 2D, and S2A). To address the relationship between ephrin and FGF inputs, we modelled the activation status of ERK by both SOS (downstream of FGF/FGFR signals) and p120RasGAP (downstream of ephrin/Eph signals) (Figures 3D and S4A). In our simple model, Ras-GDP is transformed into Ras-GTP at a rate V_1, mediated by SOS following Michaelian kinetics. Ras-GTP is converted back into Ras-GDP by two different processes: one mediated by p120RasGAP following Michaelian kinetics with a rate V_2 and the other mediated by ephrin- and cell surface contact-independent GAP activity with a linear rate k_b. We evoked the presence of basal GAP activity since transcriptome datasets (Brozovic et al., 2018) indicate the presence of at least three further RasGAPs in the early ascidian embryo (*IQGAP1/2/3*, *Neurofibromin*, *RASA2/3*). We assume that Ras-GTP activates ERK with a Hill relationship and that the total amount of Ras-GDP and Ras-GTP is conserved. So, we only consider the fraction of Ras-GTP:

$$\text{i.e. } \frac{[Ras-GTP]}{[Ras-GDP]+[Ras-GTP]} \text{, called T.}$$

The fraction of Ras-GDP = 1-T. Similarly, we consider the normalized ERK activity, called Erk*, which represents the ERK activity divided by the maximal possible ERK activity.

The evolution equation for T is given by:

$$\frac{dT}{dt} = V_1 \frac{(1-T)}{K_1+(1-T)} - V_2 \frac{T}{K_2+T} - k_b T \qquad (1)$$

This equation is solved at equilibrium to get the value of T for different values of V_1, V_2 and k_b. The fraction of active ERK is also assumed to be at equilibrium and is given by:

$$Erk^* = \frac{T^2}{K_{erk}^2+T^2} \qquad (2)$$

The Hill coefficient of 2 reflects potential moderate cooperativity in the ERK activation pathway (see Figure S4A for similar results with Hill=1).

Varying V_1, V_2 and k_b, this model, which depends on the presence of an ephrin-independent RasGAP activity, fits well with experimental observations (Figures 3D and S4A). Activation of ERK depends on SOS, consistent with the strong down regulation of ERK when FGF signals are inhibited (Figures 2A, S1D, and S1F-S1H) (Hudson et al., 2016; Kim and Nishida, 2001; Nishida, 2003; Picco et al., 2007). At high p120RasGAP activity levels, ERK is strongly suppressed at all levels of SOS activity. This is consistent with the repression of ERK and ERK-dependent cell fates when ephrin ligands are overexpressed (Haupaix et al., 2013; Ohta and Satou, 2013; Picco et al., 2007). At fixed (medium to high) SOS activity, differential p120RasGAP alone can generate a wide range of ERK values, as previously shown (Ohta et al., 2015). Similarly, at fixed (medium to low) p120RasGAP activity, differential SOS can generate a wide range of ERK activity, consistent with our data (Figures 2C, 2D, S1C, and S2A). Thus, the model predicts that either differential SOS or differential p120RasGAP (in the presence of SOS) is capable of creating differential ERK activity across a field of cells, while changing SOS generates a greater spread of ERK activation levels compared to changing p120RasGAP. This indicates that differences in the cell contact surfaces with FGF-expressing mesendoderm cells would have a greater impact on ERK activation levels than that with ephrin-expressing ectoderm cells. Furthermore, the optimum spread of ERK activation levels takes place when both FGF and ephrin/Eph signals are differential (i.e. a diagonal line across the graph). Thus, an inductive system with two antagonistic signals exhibits a greater dynamic range of responses. It is likely therefore that both differential FGF- and ephrin-signaling inputs contribute to the embryonic pattern of ERK activity during early neural induction.

Mathematical analysis indicates greater sensitivity to changes in cell surface contact compared to changes in ligand concentration

Our data suggest that the area of cell surface contact is a strong determinant for the differential pattern of ERK activation observed between the different a-line cells. In this scenario, the area of cell surface contact is proportional to the number of FGF receptors that are exposed to a uniform concentration of FGF ligands (Figure 4A). This is conceptually different to a classical morphogen gradient scenario, whereby cells are exposed to different concentrations of ligands. The neural induction scenario (Figure 4A) implies a uniform density of FGFR at the membrane of the different a-line cells. We were unable to measure

the density of endogenous FGFR at the membrane. However, exogenously supplied FGFR was evenly distributed between a-line cells and was able to recover differential ERK activation between a-line cells in FGFR-depleted embryos (Figures 4B and S4B). Models predict that ephrin signaling alone, in the presence of uniform SOS activation, can generate a differential pattern of ERK activation among a-line cells (Figure 3D) (Ohta et al., 2015). Therefore, we conducted this experiment in the presence of NVP to inhibit ephrin/Eph signals. Endogenous *FGFR* was knocked-down with morpholino (FGFR-MO) injection into unfertilized eggs. At the 8-cell stage, *FGFR-Venus* mRNA was injected into one a4.2 cell and dpERK levels were quantified at the late 32-cell stage (Figure 4B). On the *FGFR-Venus* injected side of the embryo, a6.5 exhibited the highest dpERK levels in 95% of cases (Figure 4B). Furthermore, the exogenously-provided FGFR restored a a6.5>a6.7>a6.6>a6.8 pattern of ERK activation in 30% of embryos (6/20) with the average dpERK profile similar to that obtained for sibling NVP-treated embryos (Figure S4C).

This suggests that differential cell surface contact with even FGFR densities is sufficient to generate a differential pattern of ERK activation between a-line cells and select a6.5 as the cell with the highest ERK activity.

ERK activation levels also depend on the concentration of FGF ligands to which FGFR are exposed (Figures 3B and 3C). Using a mathematical analysis, we investigated the respective importance of the extracellular concentration of FGF and receptor numbers in determining the differential pattern of ERK activation. We first adopted a simple model to address the role of the FGF signal input alone. We assume that the density of the FGFR is the same for all cells, FGF acts as a short-range ligand, and the extracellular concentration of FGF, [Fgf], between the mesendoderm cells and the ectoderm cells is constant. Thus, [Fgf] is the same for all cells, but the number of active FGFR is different from one cell to another, because the area of surface (i.e number of FGFR) exposed to the ligands is different (Figure 4A). These assumptions are entirely consistent with experimental data (this study) (Guignard et al., 2020; Miyazaki et al., 2007; Tassy et al., 2006).

The effective input into the ERK cascade is the number of receptors bound to FGF (R_B, for bound receptors), which can be expressed as:

$$R_B = R.\frac{[Fgf]}{[Fgf]+K_d} \qquad (3)$$

where R is the number of receptors in contact with FGF-expressing cells and K_d the binding constant of FGF to its receptor. A non-cooperative relation (n_H=1) is taken in which one FGF binds to one FGF receptor as used previously (Blum et al., 2019; Guignard et al., 2020). The ERK signaling cascade is assumed to be non-linear, so the relationship between ERK activity (Erk^A) and bound receptors (R_B) is non-linear:

$$Erk^A = Erk_{max}\frac{R_B^n}{R_B^n + K_{DR}^n}$$

where Erk_{max} is the maximal cellular ERK activity, and K_{DR} is the number of FGF-bound receptors leading to half maximal activity (in a.u.). One can define a normalized ERK activity as

$$Erk^* = \frac{Erk^A}{Erk_{max}} = \frac{R_B^n}{R_B^n + K_{DR}^n} \qquad (4)$$

Inserting (3) into (4) gives

$$Erk^* = \frac{R^n\left(\frac{[Fgf]}{[Fgf]+K_d}\right)^n}{R^n\left(\frac{[Fgf]}{[Fgf]+K_d}\right)^n + K_{DR}^n} \qquad (5)$$

Measurements of ERK activity as a function of cell surface contact describe ERK activity as a function of R. Our experiments revealed a strong correlation in this relationship (Figures 2D and S2A). Curve fitting with a best-fit Hill function of this relationship generate Hill coefficients greater than 1, suggesting some degree of ultrasensitivity (Figure S2A). For the mathematical analysis, we took Hill coefficients of 2.6, 2.0 and 1.6 to describe this relationship, presenting in detail the results for Hill=2.6 (Figures 4C and S4D).

From equation (5), we can see that the relation between normalized ERK activity (Erk*) and the number of receptors in contact with FGF (R) is not the same as the relationship between Erk* and [Fgf]. If we keep R constant but vary [Fgf], the Hill coefficient for the relationship between Erk* and [Fgf] never reaches 2.6 but remains smaller, with the exact value of the Hill coefficient depending on the value of R (Figures 4C and S4D). We can analytically express the relationship between the Hill coefficient of "ERK versus R" (n) and the Hill coefficient of "ERK versus [Fgf]" (n_H) (Figure S4D and STAR Methods). This shows that, for a given n, n_H is equal to or smaller than n, with the exact n_H depending on K_{DR}/R (the number of FGF-bound receptors at half maximum ERK activity/the number of receptors in contact with FGF-expressing cells).

Similar conclusions are reached if we include ephrin-signaling in our analysis. Combining our two modeling approaches described above (Figures 3D and 4C), we took our evolution equation for T (equation 1), described earlier, together with the activation of SOS by bound FGF receptors (R_B) and activation of p120RasGAP by bound Eph receptors (Q_B) (see STAR Methods for details):

$$\frac{dT}{dt} = V_s \frac{{R_B}^{n1}}{K_s^{n1}+R_B^{n1}} \frac{(1-T)}{K_1+1-T} - V_{rg} \frac{Q_B^{n2}}{Q_B^{n2}+K_{rg}^{n2}} \frac{T}{K_2+T} - k_b T \qquad (6)$$

The relationship between number of FGF receptors in contact with FGF-expressing cells (R) and number of Eph receptors in contact with ephrin-expressing cells (Q) is based on their linear relationship shown in Figure 1B. Thus, increases in R resulted in a corresponding decrease in Q and vice versa. Testing a wide range of parameter values, this analysis supports the conclusion that cells should be more sensitive to changes in cell surface contact (S1) than they would be to changes in FGF ligand concentration (Figure 4D), which is consistent with our experimental observations (Figures 3B and S2A). We therefore conclude that neural induction would be more robust to changes in [Fgf] than to changes in embryo geometry.

Semi-quantitative measurements of *Otx* transcription

The gradual (non-bimodal) nature of the ERK activation response described in the previous sections leads us to conclude that the precision of the lineage segregation between neural and epidermal fates is not controlled at the level of the ERK response. We therefore next addressed the transcriptional activation of its immediate-early gene, *Otx*.

The transcriptional activation of *Otx* was quantified as smFISH spots per nucleus at the late 32-cell stage when levels of smFISH spots in a6.5 are stable (Figures 5A, B, and S5). *Otx* expression was reduced by inhibition of FGF signaling and enhanced by inhibition of Eph signaling (Figures 5C and 5D), consistent with previous studies using non-quantitative methods (Bertrand et al., 2003; Ohta and Satou, 2013). Treating embryos with NVP resulted in ectopic activation of *Otx* in a6.7 cells, but also in a6.6 cells in 4 out of 6 experiments (in total 32/77 a6.6 cells had more than 100 spots) (Figures 5E and S6A-S6D). All expression was suppressed when embryos were treated in parallel with U0126, suggesting that inhibition of Eph signals results in ectopic activation of *Otx* primarily via activation of the MEK-ERK cascade (Figures 5E and S6A).

The *Otx* transcriptional response is bimodal

Under the conditions tested, cells appear to fall into two groups, with low smFISH *Otx* spot counts or high spot counts, suggesting a bimodal response of *Otx* to different levels of ERK activation. This idea was supported by an *ex vivo* assay in which ectodermal explants were treated with increasing doses of exogenous FGF (Figures 5F and S6E). Earlier, we showed that treating ectoderm cells with increasing doses of FGF resulted in a gradual increase in ERK activation levels, with nuclear dpERK IF signal exhibiting a unimodal distribution (Figures 3A-3C, S2H, S2I, and S3D). Under similar conditions, the response of *Otx* was strikingly different (Figures 5F and S6E). Hartigan's diptest supports a non-unimodal (at least bimodal) distribution of *Otx* spot counts in the *ex vivo* dose response experiments as well as in control whole embryos (Figures S3C and S3E). ephrin/Eph-inhibited embryos also maintained a bimodal *Otx* response despite ectopic activation of *Otx* (Figures S3F and S3G).

Further evidence for a sigmoidal relationship between the activation levels of ERK and the levels of *Otx* transcription was found using half-embryo injections. This experiment assumes that ephrin/Eph signals affects *Otx* expression only via its effect on ERK activation levels (Figures 5E and S6A). Embryos were injected with *Eph3ΔC* mRNA into one cell at the two-cell stage (Figure 6A). At the late 32-cell stage, one group of embryos was processed for *Otx* smFISH and another for dpERK IF. We therefore collected average values of both ERK activation and *Otx* transcription levels in eight different cell types (a6.5, a6.6, a6.7 and a6.8 from both control and *Eph3ΔC* halves). Plotting the mean level of nuclear dpERK IF signal, normalized to the dpERK IF signal of control side a6.8 (a6.8=0), against the mean number of *Otx* spots revealed a sigmoidal curve with best-fit Hill coefficients of 3.4, 6.5 and 10.7 in three independent experiments (Figures 6A and S6F). This suggests that *Otx* responds to different levels of ERK activation in a sigmoidal manner, consistent with a threshold response and a bimodal output.

ERF transcriptional repressor increases the sensitivity of the *Otx* transcriptional response

The bimodal transcriptional output of *Otx* does not depend upon ephrin/Eph signals (Figures 5D, S3F and S3G). We investigated other possible mechanisms that may contribute to the bimodal nature of *Otx* transcription. A minimal enhancer of the *Otx* gene, named the *Otx* a-element, contains 3 GATA and 2 ETS binding sites required for neural-specific expression in

the ectoderm lineages via Gata.a and ETS1/2 transcription factors (Bertrand et al., 2003; Rothbächer et al., 2007). Reduced binding affinities and sub-optimized spacing between these binding sites contribute to neural-specific expression (Farley et al., 2015). However, an optimized *Otx*-a-element did not drive ectopic expression in non-neural ectoderm lineages at the 32-cell stage (Figures S7A-S7D). This suggests that the sub-optimized nature of the *Otx* a-element does not account for the bimodal *Otx* transcriptional response in ectoderm lineages.

It has been shown that the ETS binding sites in the *Otx* a-element mediate repression of enhancer activity in non-neural ectoderm, indicating the presence of a repressor acting through these sites (Rothbächer et al., 2007). The ETS gene family also contains transcriptional repressors, which recognize the same binding site as the transcriptional activator ETS1/2 and whose activity is negatively controlled by ERK via nuclear export (Le Gallic et al., 1999, 2004). We identified a homologue of one such ETS-family member, *ERF2* (Yagi et al., 2003). Knockdown of *ERF2*, using ERF2-MO, resulted in ectopic activation of *Otx* in all ectoderm cells and the bimodal expression output was lost (Figure 6B).

Based on a phenomenological model, we tested the concept that competitive regulation of *Otx* expression by an activator and an inhibitor, whose activities are inversely regulated by ERK activity, would increase the sensitivity of the *Otx* transcriptional response to ERK (Figure 6C and STAR Methods). dpERK (E) controls *Otx* expression by the stimulation of an activator (Ap or phosphorylated activator; e.g. ETS1/2, in blue) and by the suppression of an inhibitor (I or unphosphorylated inhibitor; e.g. ERF2, in red) (Figures 6C and 6D). *Otx* as a function of E considers competition between the activator and inhibitor but does not consider the number of binding sites nor therefore any cooperativity between them. This analysis suggests that the inhibitor acts at low dpERK values and shifts the *Otx* response towards higher values of dpERK (Figure 6D). Moreover, in the presence of the inhibitor, the *Otx* response is more sigmoidal (higher Hill coefficient). This result was robust at a wide range of parameter values (Figure S7F). These analyses suggest that, at low levels of ERK activity, the presence of an inhibitor is necessary to suppress expression of *Otx* in non-neural precursor cells and contributes to the switch-like activity of the *Otx* response.

Recovery of wild-type *Otx* expression pattern in Eph-inhibited embryos by reduced MEK signaling

The above model indicates that it is crucial to maintain ERK activity at low levels in non-neural ectoderm cells in order to maintain *Otx* repression by ERF2. Our data suggest that ephrin/Eph signals account for this by reducing the levels of ERK activation in all a-line cells. Thus, it should be possible to recover the wild-type *Otx* expression pattern in Eph-inhibited embryos by some other means of reducing ERK activation levels. This was indeed the case (Figures 7A and S6B-S6D). NVP treatment resulted in an 'ON' state of *Otx* activation in a6.7 and sometimes in a6.6. Treatment of sibling NVP-treated embryos with low doses of U0126 resulted in recovery of the wild type pattern of *Otx* gene expression, restricted predominantly to a6.5. Thus, broadly lowering MEK activity in NVP-treated embryos is sufficient to re-establish the wild type pattern of *Otx* activation. Our data suggests that this critical function is achieved during normal embryogenesis by ephrin/Eph signals.

DISCUSSION

During ascidian early neural induction, variable FGF-signaling inputs are converted into a bimodal transcriptional output (Figure 7B). Our data support the idea that the area of the cell surface contact, or the number of FGF receptors exposed to a constant concentration of FGF ligands, is a strong determinant for the differential pattern of the ERK activation between cells (Figures 1-4) (Guignard et al., 2020; Tassy et al., 2006). Modeling predicts a greater impact of cell geometry compared to FGF-ligand concentration, which may have contributed to the highly conserved geometry of ascidian embryos over vast evolutionary times (Delsuc et al., 2018). The response of ERK to FGF appears to be gradual (non-bimodal), as has been reported in response to growth factors in other embryonic systems (van Boxtel et al., 2018; Coppey et al., 2008; de la Cova et al., 2017; Melen et al., 2005). ephrin/Eph signals act to reduce the level of ERK activation across all cells and contributes to the optimum spread of ERK outputs across a field of cells (Figures 2A and 3D). ephrin/Eph signals are critical to maintain non-neural ectoderm cells at low ERK activity, where *Otx* is repressed by an ETS family repressor, ERF2 (Figures 6 and 7). ERK-mediated transcriptional de-repression may be a common mechanism to control sharp expression boundaries of ERK immediate target genes during development (Lim et al., 2013; Melen et al., 2005). Future studies should address the interplay between ERK, ETS1/2, and ERF2 during the generation of the bimodal transcriptional output. Two TGFβ ligands, Admp and Gdf1/3-like, which

weaken *Otx* expression, may also be involved in sharpening the *Otx* transcriptional response (Ohta and Satou, 2013).

The ascidian early neural induction system is an attractively simple system; ERK activation to direct target gene activation takes place in identifiable cells within an *in vivo* multicellular context and within a single cell cycle of 30 minutes. The ERK signaling cascade is well conserved during evolution and widely implicated in embryonic development, as well as homeostasis and disease (Dorey and Amaya, 2010; Ornitz and Itoh, 2015; Turner and Grose, 2010). Thus, insights gained from studies in any one system are likely to be broadly relevant.

Limitations of the Study

We were unable to measure the distribution of endogenous FGFR at the cell membrane. Similarly, localized activation of the FGFR at the membrane where ectoderm cells contact mesendoderm cells is an assumption and remains to be demonstrated. The correlation between ERK activation levels in ectoderm cells and their area of cell surface contact with FGF-expressing mesendoderm cells, even in the absence of Eph signals, strongly suggests a causal relationship. However, this causality is not formally demonstrated and other aspects of cell morphology might be influencing ERK activation levels. The mathematical modeling is mostly qualitative. The relationships between dpERK, ETS1/2 and ERF2 in generating the bimodal activation of *Otx* remain to be fully understood.

ACKNOWLEDGEMENTS

We thank Benoit Godard (micro-wells); Christian Rouvière (custom-made java plugin for background subtraction in Image J); Alex McDougall's team (*pRN3-PH-GFP* and *Phallusia*); Remi Dumollard (NLS sequence); Delphine Dauga (manual 3D embryo reconstruction advice); Konner Winkley and Michael Veeman (semi-automated segmentation advice); Emma Farley (*Otx* enhancers); Brad Davidson (*FGFR-Venus*); Axel Duchene, Laurent Gilletta, Marie Hagström and Régis Lasbleiz (animal husbandry); Carine Barreau and Nathalie Dostatni (encouragement and discussions). The team of HY is supported by the Centre National de la Recherche Scientifique (CNRS), Sorbonne University, the Fondation ARC pour la Recherche sur le Cancer (PJA 20131200223) and the Agence Nationale de la Recherche (ANR-17-CE13-0003-01). GD is Research Director at the Belgian "Fonds National pour la Recherche Scientifique (FRS-FNRS)". RB is supported by a grant of the Interuniversity Institute of Bioinformatics in Brussels. All image acquisitions were conducted in the imaging platform PIM (member of MICA). Our imaging platform (PIM) and animal facility (CRB) are supported by EMBRC-France, whose French state funds are managed by the ANR within the Investments of the Future program under reference ANR-10-INBS-0.

AUTHOR CONTRIBUTIONS

Conceptualization: HY, CH, GD with inputs from GW, SdD, CS, NH, RB. Methodology: HY, CH, GW, CS, GD, SdD. Software: RB, SdD, GD. Validation: GW, SdD, CS, NH, RB, GD, CH, HY. Formal Analysis: CH, GW, HY, GD, SdD, CS, RB. Investigation: GW, HY, CH, SdD, CS, GD, NH, RB, KI, YS. Writing-original draft: CH with essential input from HY, GD. Writing- Review and editing: all authors. Visualization: CH, HY, GW, SdD, GD, CS, RB. Funding acquisition: HY, CH. Supervision: HY, CH, GD, SdD. Project administration: HY.

DECLARATION OF INTERESTS

The authors declare no competing interests**.**

FIGURE LEGENDS

Figure 1. Quantitative measurement of cell surface contact and ERK activation levels in ectoderm cells. In this and all subsequent figures, a-line cell identity is indicated by colors, with a6.5 in magenta, a6.6 in green, a6.7 in blue and a6.8 in grey. A) Left: 32-cell stage embryo reconstructed with Amira software from a confocal z-stack, a-line cells colored as described above with mesendoderm in yellow and b-line ectoderm in white. Dotted line= line of sagittal section (next panel). Scale bar is 40μm. Insert: confocal section of *PH-GFP* mRNA injected and α-GFP IF stained embryo used for reconstruction. Middle: sagittal section highlighting cell surface contacts between ectoderm and mesendoderm cells. Right: schematic drawing of interplay between FGF and ephrin/Eph signals, leading to ERK activation and *Otx* transcription. B) Left: same embryo as A with ectoderm cells removed to reveal cell surface contacts between ectoderm and mesendoderm cells; a-line contacts are colored only on the right side of the embryo. Middle: relative area of a-line cell surface contact with A-line mesendoderm cells (surface contact with A-line/total cell surface). Two tailed paired t-tests compare each cell-type per half embryo based on the hierarchical order of measurements (i.e. a6.5 to a6.7, a6.7 to a6.6, and a6.6 to a6.8), ****P<0.0001. Right: relative area of a-line cell surface contact with A-line mesendoderm cells versus ectoderm cells with Pearson correlation, R^2=0.98. C) Snapshots of Imaris 3D visualizations of confocal stacks of dpERK IF (left) and Histone H3 (middle) of the same 32-cell stage embryo. Right: a-line nuclei segmented based on H3 IF signal (colored). D) Mean pixel intensity of nuclear dpERK IF signal in a-line cells. Two tailed paired t-tests per embryo half compare a6.5 to a6.7, a6.7 to a6.6, and a6.6 to a6.8. ****P<0.0001. E) Relative area of cell surface contact with A-line cells and mean pixel intensity of nuclear dpERK IF signal in individual a-line cells, with Spearman correlation. F) ERK-KTR in *P. mammillata embryos*. Time-lapse movies were normalized to t=0 at the point of A6.4 nuclear envelope breakdown (NEBD). Left: time-lapse still, a-line cells highlighted with a red dotted line with positions of their nuclei indicated on the drawing. Middle: log2 ERK-KTR cytoplasmic/nuclear (C/N) ratio for each cell type at late 32-cell stage (t= 6'). Two tailed paired t-tests per embryo half compare a6.5 to a6.7, a6.7 to a6.6, and a6.6 to a6.8. ****P<0.0001, *P<0.05, ns P≥0.05. Right: log2 (C/N ratios) of cells normalized to the same side a6.8 C/N ratio (=1) during the 32-cell stage, each line represents

a single cell. B, D, E, F) For graphs, each dot represents a single cell, colored according to a-line code, bar=mean. In B (middle), D and F (middle), the dotted line and percentages represent the percentage of half embryos in which a6.5>a6.7, a6.7>a6.6 and a6.6>a6.8. See also Figures S1-S3.

Figure 2. ERK activation in FGF- and Eph- signal inhibited embryos. A) Left: experimental procedure. Graph shows injected/control ratios of mean pixel intensity of nuclear dpERK IF signal for each cell type in *PH-GFP*, *dnFGFR, Eph3ΔC* and *RGΔGAP* injected embryos. Number of ratios analyzed for each cell-type indicated in parentheses (below). Statistical tests are one sample two-tailed t-tests with a theoretical mean of 1. ****P<0.0001, **P<0.01, *P<0.05, ns P≥0.05. B) Left: experimental procedure. Middle: ectopic activation of ERK in a6.7 on the injected side of all 9 embryos confirmed the efficiency of *Eph3ΔC* (injected cells outlined). Right: paired two tailed t-tests compare each cell type between control (C, ●) and injected (inj, ▲) halves, ns P≥0.05. C) Mean pixel intensity of nuclear dpERK IF signal in NVP-treated embryos. Two tailed paired t-tests compare in each half embryo a6.5 to a6.7, a6.7 to a6.6, and a6.6 to a6.8, ****P<0.0001. The dotted line and percentages represent the percentage of half embryos in which a6.5>a6.7, a6.7>a6.6 and a6.6>a6.8. D) Relative area of a-line cell surface contact with A-line cells and mean pixel intensity of nuclear dpERK IF signal in NVP-treated embryos, with Spearman correlation. For all graphs, each dot represents a single cell, colored according to a-line code, bar=mean. See also Figures S1-S3.

Figure 3. ephrin/Eph signaling modifies the amplitude and dynamic range of ERK responses. A) Experimental procedure for *ex vivo* analysis of ERK activation responses. B) Normalized α-dpERK signal (mean $\pm$ SD) of 12 pairs of western blots showing dose response to exogenous bFGF in control and NVP-treated explants. n_H: best-fit Hill coefficient. C) Mean pixel intensity of nuclear dpERK IF signal in ectodermal explants treated with increasing doses of bFGF. Each dot represents a single cell, orange bar = mean. we= mean nuclear dpERK IF signals of a-line cells of control whole embryos processed in the same tubes as explants. n=number of cells analyzed in explants per dose of bFGF. D) Left: mathematical modeling scheme of ERK activation integrating SOS (V_1), p120RasGAP (V_2) and basal RasGAPs activities (k_b). Right: model output of ERK activity at k_b =0.2. Below the graph are circles depicting six cells spread evenly across the graded activities of SOS and p120RasGAP at three

different positions (white circles on the graph), (**a**) differential SOS with no p120RasGAP (FGF only); (**b**) differential p120RasGAP with no SOS (ephrin only); and (**c**) both differential SOS and differential p120RasGAP (FGF + ephrin). $K_{erk} = K_1 = K_2 = 0.5$. See also Figures S2-S4.

Figure 4. Mathematical analysis indicates that ERK responds with higher sensitivity to changes in cell surface contact than to changes in FGF concentration. A) Schematic representation of cell-contact based signaling, following the key on the right: nuclei in grey circles with shading depicting different levels of ERK activation. B) Top: experimental procedure. Below are snapshots of Imaris 3D visualizations of confocal stacks of Histone H3 and dpERK IF of the same 32-cell stage embryo. In this FGFR-MO injected embryo, the a6.5>a6.7>a6.6>a6.8 pattern of dpERK IF signal was restored by *FGFR-Venus* mRNA injection. *FGFR-Venus* injected cells outlined with white dotted line with a grey solid line outlining the entire embryo. Right: graph shows mean+SEM for each a-line cell mean pixel intensity of nuclear dpERK IF signal. Two tailed paired t-tests on embryo halves compare the cell types indicated by brackets, ****P<0.0001, ** P< 0.01, *P<0.05, ns P≥0.05. Percentages represent the number of half embryos in which a6.5>a6.7, >a6.6 or >a6.8 (pink), a6.7>a6.6 or >a6.8 (blue) or a6.6>a6.8 (green) as indicated by brackets. No statistical difference was observed between any cells from the non-rescued half of the embryo. C-D) Mathematical analysis following the neural induction scenario. C) Left: ERK as a function of R (number of receptors in contact with FGF-expressing cells) following equation (5) (see text) with a Hill coefficient n=2.6. Right: equation (5) solved to show Erk* as a function of changing FGF concentration with n=2.6, K_d=100nM and at fixed R (R=1000 (blue line), 750 (orange), 500 (yellow) and 250 (purple)) with their corresponding Hill coefficients n_H. D) Graphs showing the Hill coefficients obtained from further modeling considering also ephrin/Eph signals (see STAR Methods for details). ERK responses show higher sensitivity to changes in surface contact (S1) compared to changes in FGF ligand concentration ([Fgf]) over a wide range of parameter values. See also Figure S4.

Figure 5. **Bimodal expression of *Otx*.** A) Imaris segmented nuclear *Otx* smFISH spots (red) in a control embryo, with DAPI (white). a-line cells are highlighted with a red dotted line and their nuclear positions indicated on the drawing (right). B-F) smFISH *Otx* quantification in late 32-cell stage embryos or explants, each dot represents a single cell. B) Two tailed paired

t-tests compare a6.5 to a6.7, a6.7 to a6.6, and a6.6 to a6.8 in control embryos pooled from 4 independent experiments (indicated by different shades/shapes of spots), ****P<0.0001, *** P< 0.001, ns P≥0.05. Black bar=mean. C) Experimental procedure for D. D) Two tailed paired t-tests compare each cell-type between control and injected halves. Only statistically significant tests are shown with a6.5 paired comparisons in pink and a6.7 paired comparisons in blue. ****P<0.0001, ***P<0.001. E) Control, NVP- and NVP- plus U0126-treatment. F) Ectodermal explants treated with increasing doses of bFGF and analyzed for smFISH *Otx*. See also Figures S3, S5, and S6.

Figure 6. ERF is required for the spatial precision of the *Otx* transcriptional response. A) Top: experimental design. Graph: Mean and SEM of each cell type in control (●) and *Eph3ΔC*-injected (■) half embryos from two groups of embryos, one group in which mean dpERK IF signal was measured and normalized by subtracting mean control side a6.8 signal (a6.8 = 0) and one group in which *Otx* smFISH spots were counted. Best-fit Hill coefficient following curve fitting = 6.5 (95% confidence interval 3.4 to upper limit could not be calculated). B) smFISH *Otx* of control-MO and ERF2-MO injected embryos. Top: Imaris segmented nuclear *Otx* smFISH spots (red), with DAPI (white). Graph with unpaired two-tailed t-tests comparing each cell type between the two groups: ****P<0.0001, **P<0.01. Each dot represents a single cell, bar=mean. C) Mathematical modeling scheme for the actions of a competitive activator (Ap) and inhibitor (I) on *Otx* transcription. D) Model outputs. Left: fraction of phosphorylated activator (Ap) and non-phosphorylated inhibitor (I) as a function of dpERK (E). Right: *Otx* as function of dpERK (E) in the presence (blue line) and absence (orange line) of I. See also Figures S7.

Figure 7. *Otx* spatial precision depends on Eph-mediated dampening of ERK activity. A) Recovery of control *Otx* expression pattern in NVP-treated embryos with low doses of U0126; each dot represents a single cell. Top: Imaris segmented nuclear smFISH *Otx* spots (red) in examples of control, NVP- and NVP- plus low dose U0126- treated embryos, with DAPI (white). *Otx* spot counts were re-tabulated based on treatment and cell-type for 2-way ANOVA analysis comparing each experimental sample to control (**** P<0.0001; ns, P≥0.05). B) Visual summary of variable FGF-signal input (or R) to bimodal *Otx* output. Heatmaps are data from Figure 1B, and the first 26 embryos from Figure 1D and Figure 5B.

Heatmap scale limits are set as follow (FGF input: 0.025 to 0.45; dpERK: 114 to 736; *Otx* 0.1 to 607).

STAR METHODS

RESOURCE AVAILABILITY

Lead Contact

Further information and requests for resources and reagents should be directed to and will be fulfilled by the Lead Contact, Hitoyoshi Yasuo (yasuo.hitoyoshi@imev-mer.fr).

Materials Availability

Modified plasmids generated in this manuscript will be shared upon request to the lead contact.

Data and Code Availability

Matlab/python codes developed for all modeling are available on request.

EXPERIMENTAL MODEL AND SUBJECT DETAILS

Experimental Model

Adult *Ciona intestinalis* and *Phallusia mammillata* were purchased from the Station Biologique de Roscoff (France) and the Station Marine de Sète (France), respectively, and maintained in running sea water. All experiments were conducted with *C.intestinalis* except ERK-KTR experiments, which were conducted with *P.mammillata*.

METHOD DETAILS

Ascidian embryo culture and basic methods

Ascidian embryo culture (Hudson, 2020; Sardet et al., 2011), microinjection (Sardet et al., 2011; Yasuo and McDougall, 2018) and electroporation (Hudson et al., 2016) have been described. Cell names, lineages and fate maps were described previously (Conklin, 1905; Nishida, 1987). For detection of *Venus* transgene driven by 69-WT and 49-Opt *Otx* enhancers (Farley et al., 2015), digoxigenin-labelled *Venus* probes were used in the *in situ*

hybridization protocol described in (Hudson, 2020). The late 32-cell stage was defined visually under binocular microscope, as when vegetal cells "decompact" and embryos become flattened in shape, corresponding to approximately 5-7 minutes before vegetal cells exhibit the first sign of cytokinesis.

Ciona robusta Gene Model IDs

We use *C.robusta* (*C. intestinalis type A*) gene model IDs (Satou et al., 2008) as the genome of *C. robusta* currently has better annotation compared to *C. intestinalis* (*C. intestinalis type B*) (Satou et al., 2019).

FGF9/16/20: KH2012:KH.C2.125

M-Ras: KH2012:KH.L172.2

ERK1/2: KH2012:KH.L153.20

MEK1/2: KH2012:KH.L147.22

FGFRc: KH2012:KH.S742.2

Efna.d: KH2012:KH.C3.716

Eph3 (now called Eph.c): KH2012:KH.C7.568

Otx: KH2012:KH.C4.84

p120RasGAP (also known as RASA1): KH2012:KH.L152.46

IQGAP: KH2012:KH.L87.13

Neurofibromin: KH2012:KH.L109.6

RASA2/3: KH2012:KH.C1.339

ETS1/2: KH2012:KH.C10.113

Gata.a (Gata4/5/6): KH2012:KH.L20.1

ERF2: KH2012:KH.C4.366

For other components of the FGF signaling pathway, refer to: (Brozovic et al., 2018; Satou et al., 2003: Satou et al., 2005).

Molecular tools

pRN3-PH-GFP was reported previously (Carroll et al., 2003; Prodon et al., 2010) and mRNA was injected at concentration of 1.5μg/μl. *pRN3*-dn*FGFR* was reported previously (Hudson et al., 2007) and mRNA was injected at a concentration of 1 μg/μl. *pRN3-RGΔGAP* is described previously (Haupaix et al., 2013) and mRNA was injected at a concentration of 1.5μg/μl.

pRN3-Eph3ΔC was described previously (Picco et al., 2007) and was injected at a concentration of 1.25μg/μl. *pSPE3-ERK-KTR-mClover* was generated by a Gateway reaction of *pSPE3-RfA* (Roure et al., 2007) and *pENTR-ERKKTRClover* (Regot et al, 2014) and mRNA was injected at a concentration of 1.5μg/μl together with *NLS-tdTomato* mRNA at 3μg/μl. *NLS-tdTomato* mRNA was synthesized from *pRN3-NLS-tdTomato* consisting of a single N-terminal *NLS* (5'-ATGACTGCTCCAAAGAAGAAGCGTAAGGTA-3') fused to the *tdTomato* ORF. *pRN3-FGFR-Venus* was constructed by subcloning the PCR-amplified *FGFR-Venus* ORF from *Mesp>FGFR-Venus* (Cota and Davidson, 2015) into pRN3 (Lemaire et al., 1995). *FGFR-Venus* mRNA was injected into the right a4.2 cell of 8-cell stage embryos at a concentration of 0.5μg/μl for visualization at the basolateral membrane by α-GFP IF or at 0.01-0.04μg/μl for the rescue of FGFR-MO embryos. *pRN3-ERF2* was constructed by subcloning PCR-amplified *ERF2* ORF from *pENTR-ERF2* (Gilchrist et al., 2015) into pRN3 and *ERF2* mRNA was injected at a concentration of 0.25μg/μl. All mRNAs were synthesized using mMESSAGE mMACHINE T3 kit (Invitrogen/ Thermo Fisher Scientific, Massachusetts, USA).

69-WT and 49-Opt *Otx* enhancers (Farley et al., 2015) were cloned upstream of bpFOG-Venus based on the Gibson Assembly method (Gibson et al., 2009). Morpholinos were purchased from GeneTools (Philomath, Oregon): FGFR-MO (5'-GTATCATTTTTTCTACCCTAATCAC-3'); ERF2-MO (5'-CATAATTAAGTCTTTGATAACAACG-3') and Control-MO (Msx-MO: 5'-ATTCGTTAACTGTCATTTTTAATTT-3' (Esposito et al., 2017)) were injected at a concentration of 0.5mM into unfertilized eggs and incubated overnight. U0126 (Calbiochem/Merck, Darmstadt, Germany) was diluted into sea water at a concentration of 2μM, unless otherwise stated. NVPBHG712 was purchased from Tocris Bioscience (Bristol, UK) or Sigma-Aldrich (Missouri, USA) and used at a concentration of 4μM (Western blots) or 6-8μM (embryo analysis), determined empirically. Dextran-tetramethylrhodamine (TRITC) or -Fluorescein isothiocyanate (FITC) (ref: D1868 and D1821, Invitrogen/Thermo Fisher Scientific, Massachusetts, USA) was made to 50mg/ml in water, and injected at 1/4 dilution.

Immunofluorescence (IF)

For embryos in which we visualized the cell surface contacts alone (Figures 1A, 1B, and S1B), we used 3.2% PFA-Seawater fix for 30 mins at RT. For detection of FGFR-Venus in embryos

injected with *FGFR-Venus* mRNA in the right a4.2 (Figure S4B), embryos were first dissected along a parasagittal line with a glass needle at mid-32-cell stage so that the a6.5 and a6.6 basal membranes are positioned at a similar depth relative to the edge of the embryo and allow us to later position the labelled cells close to the objective for the confocal acquisition. Injected halves were fixed in 3.2% PFA-Seawater for 30 mins at RT. For anti-dpERK IF, embryos were fixed at the late 32-cell stage in PIPES-Sucrose-PFA fix with 0.05% Triton-X (Stolfi et al., 2011) for 25 minutes at RT. All fixed embryos were subsequently treated by the same IF protocol. Fixative was gradually replaced with PBS-0.1% Triton followed by washes (3 times 10 minutes). Blocking was carried out for 30 minutes in PBS-Triton-0.5% Blocking Reagent (ref: 11096176001, Roche/Sigma-Aldrich, Missouri, USA). Embryos were then placed in the blocking buffer plus antibodies overnight at 4°C. For anti-dpERK IF, we used at 1/100, either anti-phospho ERK1/2 (Thr202/Tyr204) mouse monoclonal antibody (4B11B69) (ref: 675502, lot: B196626, Biolegend, California, USA) or anti-phospho-ERK1/2 (Thr202/Tyr204) mouse monoclonal antibody (MILAN8R) (ref: 14-9109-80, lot: 2350233, eBioscience/ThermoFisher, Massachusetts, USA). For anti-H3 IF, we used anti-Histone H3 XP rabbit monoclonal antibody(D1H2) (ref: 4499T, Cell Signaling Technology, Massachusetts, USA) at 1/100. Goat-anti-GFP (ref: ab5450, abcam, Cambridge, UK) was used at 1/250. Following the overnight incubation in primary antibodies at 4°C, embryos were washed in PBS-0.1% Tween (3 times 30 minutes) and then placed in PBS-Tween-0.5% Blocking Reagent (Roche) containing corresponding secondary antibodies: Alexa Fluor 555 donkey anti-goat IgG (H+L) cross-adsorbed secondary antibody (ref: A-21432, Invitrogen/Thermo Fisher Scientific, Massachusetts, USA); Alexa Fluor 488 donkey anti-rabbit IgG (H+L) (ref: 711-545-152, Jackson ImmunoResearch, Pennsylvania, USA); Alexa Fluor 647 donkey anti-mouse IgG (H+L) (ref: 715-605-150, Jackson ImmunoResearch, Pennsylvania, USA) at 1/250 for 2 hours at RT (in the dark), followed by washes in PBS-Tween, 3 times 1 hour at RT and overnight at 4°C. In half embryo injections using FITC-dextran (Figures 6A and S6F), anti-H3 was detected by goat anti-rabbit IgG (H+L) secondary antibody conjugated with Alexa Fluor 555 (ref: A-21429, Invitrogen) and anti-dpERK was detected by goat anti-mouse Alexa Flour 647 (ref: 115-605-003; Jackson ImmunoResearch).

In one experiment, shown in Figure 2B, non-quantitative anti-dpERK IF based on tyramide signal amplification was used as described (Haupaix et al., 2013; Stolfi et al., 2011). For membrane staining, embryos were incubated in Alexa Fluor 488 phalloidin in PBS-Triton

(2 units/100µL, Life Technologies, A12379) overnight at 4°C and washed in PBS-Triton (3 times, 5 min) (Robin et al., 2011a).

Image acquisition of IF-labelled embryos

For confocal observation of membrane staining alone of *PH-GFP* injected and α-GFP IF stained embryos (Figure 1A-B), embryos were individually mounted in 1% methylcellulose in PBS and scanned using AOTF linear compensation with an HCX PL APO 63x/1.2 water immersion objective on a Leica SP5 confocal microscope (Leica, Wetzlar, Germany) with a z-step of 0.3µm at 512 x 512 pixels (205.4 x 205.4 microns), 8 bits per pixel. For confocal observation of *FGFR-Venus* injected embryos stained for anti-GFP IF, embryos were individually mounted in Citifluor AF1 (Electron Microscopy Sciences, Hatfield, Pennsylvania) with their sagittal section facing to the coverslip and scanned with an HCX PL APO 63x/1.4-0.6 oil immersion objective on a Leica SP5 confocal microscope with a z-step of 0.75µm at 512 x 512 pixels (82 x 82 microns), 12 bits per pixel.

For all dpERK IF experiments, embryos or explants from a single experiment were aligned on a single poly-L-lysine coated coverslip for a single acquisition session. Embryos/explants in PBS-Tween were aligned manually by sticking onto the coverslip in rows; embryos were stuck with animal pole side up when membrane staining was also required (Figures 1E, 2D and S2A), or down for all other experiments. Aligning embryos was carried out in a small volume of methylcellulose (1% in PBS) placed on the coverslip to prevent embryos falling onto the coverslip by gravity. For confocal observation of membranes in *PH-GFP*-injected embryos stained with α-dpERK/α-GFP/α-H3, we first cleared embryos aligned on a coverslip with progressive concentrations of SeeDB (20%, 40%, 60%, final 80%) (Ke et al., 2013). The coverslip was then mounted with spacers (strips of coverslip n°1) on a slide in 80% SeeDB followed by acquisition with a HCX PL APO 63x/1.4-0.6 oil immersion objective on a Leica SP5 confocal microscope (Leica, Wetzlar, Germany) with a z-step of 0.3µm at 512 x 512 pixels (164 x 164 microns), 8 bits per pixel. For subsequent acquisition of anti-dpERK and H3 IF images, the slide was placed in a petri dish filled with PBS and the coverslip was gently recovered from the slide. The coverslip was then incubated twice for 5 minutes in 100% methanol, before mounted in a drop of benzyl alcohol:benzyl benzoate (BABB) 2:1 (Azaripour et al., 2016; Dent et al., 1989) on a slide with spacers (strips of coverslip n°1). The anti-dpERK and anti-H3 signals were then acquired using an HCX PL

APO 63x/1.4-0.6 oil immersion objective on a Leica SP5 confocal microscope with a z-step of 1μm, at 512 x512 pixels (136.7 x 136.7 microns), 12 bits per pixel. Confocal lasers were adjusted between control and NVP-treated embryos in order to obtain maximum range around the different intensities unless stated that samples were processed under identical (same tube) conditions, in which case acquisition was carried out under the same settings in the same session. In experiments that included injection of lineage tracer (dextran-TRITC or -FITC), a snap shot was taken to identify the injected cells.

For the experiment shown in Figure 2B, embryos were attached to poly-L-lysine-coated coverslips. Coverslips were then immersed in isopropanol series (5 min in 20%, 40%, 60%, 80%, 2x100%) and finally embryos were cleared in BABB. Coverslips were mounted on a slide with spacers and embryos were imaged with a HCX PL APO 63x/1.4-0.6 oil immersion objective on a Leica SP5 confocal microscope (Leica, Wetzlar, Germany). Z steps were set at 2μm.

ERK-KTR

The biosensor ERK-KTR is comprised of an ERK docking site, a bipartite nuclear localization signal (bNLS), and a nuclear export signal (NES), with ERK phosphorylation sites located within the bNLS and NES (Regot et al., 2014). For live imaging, we used *Phallusia mammillata* embryos (which belong to the same order, Phlebobranchia, as *Ciona*) for their transparency and efficiency with which they translate injected mRNA (Delsuc et al., 2018; Prodon et al., 2010). *ERK-KTR-mClover* mRNA (Regot et al., 2014) was injected into eggs together with *NLS-tdTomato* mRNA for nuclear identification. Injected eggs were incubated at least for one hour before fertilization. After fertilization, embryos were left to develop until the 16-cell stage, then placed in a glass bottom dish covered with multi-microwells made with MY-134 polymer (My Polymers Ltd, Nes-Ziona, Israel) (Engl et al., 2014) and coated with 0.1% gelatin. Embryos were placed in wells so that a-line ectoderm cells were facing directly to the coverslip. Multi-position live-imaging was carried out with a HC PL APO 40x/1.10 water immersion objective on a Leica SP5 confocal microscope. The embryo shown in Figure 1F was slightly squashed to the coverslip on its ectoderm side so that the nuclei of all a-line cells could be captured within the same confocal z-sections. Stacks were acquired every 2 minutes with a z-step of 2μm at 256 x 256 pixels (155 x 155 microns), 8 bits per pixel.

***Ex vivo* FGF dose response**

For the *ex vivo* experiments, embryos were bisected at the 8-cell stage into ectoderm (animal) and mesendoderm (vegetal) halves and cultured in BSA-ASW (artificial sea water) in petri dishes as described (Hudson and Lemaire, 2001). Since early neural induction occurs during the 32-cell stage of development, we started FGF-treatment soon after the ectoderm cells have divided at the very early 32-cell stage. Sibling embryos exited the 32-cell stage approximately 25 minutes later with cytokinesis of the vegetal cells. For NVP-treatment, explants were placed in 4μM NVPBHG712 when sibling embryos reached the late 16-cell stage. Explants and embryos from the same fertilization were observed under dissection microscope until ectoderm cells started dividing towards the 32-cell stage, then placed in various concentrations of bFGF (FGF-2) (ref: F-0291, Sigma-Aldrich, Missouri, USA).

In order to assure precise fixation times, the final minutes of incubation were carried out directly in the preparation tubes. For anti-dpERK IF, samples were fixed and processed as described above. For western blot, samples were processed as follows.

Western blot

In the preparation tube containing explants, ASW was removed to 5μl and 5μl of 2x Laemmli buffer (1.25mM Tris.HCl pH6.8, 20% glycerol, 4% SDS, 0.1% Bromophenol blue, 200mM DTT) was added, vortexed and boiled for 2 minutes. To be within the linear range of both primary antibodies (anti-dpERK and anti-PKCζ), between 6 and 10 explants were collected per tube. On every gel, a standard dilution series of whole 32-cell stage embryo sample was loaded to ensure that all samples were within the linear range for the two antibodies used. This was also used to normalize the signal between gels, as described below (Western blot quantification).

Samples were loaded with standard molecular weight markers onto 12% precast polyacrylamide gels (Mini-Protean TGX^{TM} gels, ref: 4561046, Biorad, California, USA) and migrated under standard conditions. Transfer was carried out onto PVDF membrane (Hybond™ P0.45, ref: 10600023, Amersham/Sigma-Aldrich, Missouri, USA) under standard conditions with a Biorad wet electroblotting system for 2 hours at 60 volts, with ice pack and stirrer. For antibody economy, the membrane was cut between the 28 and 130 kDa markers. Membrane was rinsed in TBS-0.1% Tween, then the same solution with 5% milk powder for 1 hour at RT. Membranes were placed in the milk solution with 1/1000 rabbit anti-dpERK

(D13.14.4E) (ref: 4370, lot: 15 and 17, Cell Signaling Technology) and 1/1000 rabbit anti-protein kinase C zeta type (PKCζ) (C-20) (ref: sc-216, Lot: B0810, Santa Cruz Biotechnology, Texas, USA), sealed in plastic bags and gently rocked overnight at 4°C. After washes in TBS-Tween, membrane was placed in 5% powdered milk solution with 1/10000 goat anti-rabbit-HRP (ref: 111-035-144, Jackson Immunoresearch) for two hours at RT followed by TBS-Tween washes. Western blots were revealed with SuperSignal West Femto Maximum Sensitivity Substrate (ref: 34095, Thermo Fisher Scientific) according to manufacturer's instructions, using the Fusion FX ECL machine (Vilber Lourmat, Collegien, France) and Fusion Software. For both dpERK and PKCζ, a linear range of between one and 10-12 (i.e. at least 10-fold) whole embryos could be obtained under these conditions. In the 16-bit images obtained for each western blot for each signal (dpERK and PKCζ), some saturation was tolerated at high embryo load in the linear range to get the best possible signal range around the samples (in which no saturation was tolerated).

We first tested the temporal response of ectoderm cells to bFGF-treatment. Levels of dpERK first peaked at around 6-9 minutes before stabilizing at around 15-24 minutes (Figures S2D and S2E). This profile of ERK activation with an excitation peak before steady state is similar to that seen in mammalian cell culture systems (Ahmed et al., 2014; Blum et al., 2019; Regot et al., 2014; Ryu et al., 2015). The entire temporal response was sensitive to Eph inhibition (Figure S2E). For the dose response, a test was conducted for control ectoderm explants collected at 9- (peak ERK) or 18- (stable ERK) minutes after addition of FGF (6 replicates collected at both time points) and processed as described below. At both time points, the dose response appeared gradual (Figure S2F). Due to the highly dynamic nature of the ERK response at 9 minutes, we decided to conduct our analysis testing the effect of Eph-inhibition ('NVP-treatment') at 18 minutes, when activation levels of ERK were relatively stable. To test the effect of Eph inhibition on the dose response kinetics of ERK at 18 minutes, for each dose response experiment (Figures 3B and S2G), explants from the same batch of embryos were treated with or without NVPBHG712, in addition to bFGF, collected for western blot and processed in parallel.

Single molecule FISH

For single molecule fluorescent *in situ* hybridization (smFISH), a commercially available kit (RNAscope® Fluorescent Multiplex Assay, Advanced Cell Diagnostics/Bio-Techne, Minnesota,

USA) with RNAscope Probe- Ci-Otx (#421381-C1) or Ci-Fgf9 (#1053651-C1) was used. Briefly, embryos were fixed at late 32-cell stage in 4% PFA, 0.5M NaCl, 0.1M MOPS, overnight at 4°C and then dehydrated in ethanol for storage. After rehydration, embryos were permeabilized in Pretreat4 (provided by the kit) for 30 min and post-fixed in 4% PFA-PBS-0.1% Tween. Probe hybridization was carried out overnight at 40°C in a water bath. Then, post-hybridization steps were conducted according to manufacturer's instructions. The last amplification step was carried out with the fluorescent label Atto 550. Nuclei were counterstained for 2 min with the DAPI solution provided by the kit. Finally, embryos were mounted and oriented one by one in Citifluor AF1 (ref: AF1-100, Biovalley France, Illkirch-Graffenstaden, France) and imaged thereafter with a HC PL CS2 63x/1.4 oil immersion objective on a Leica SP8 confocal microscope. Images were obtained with high pixel resolution (90-150nm).

In the experiment showing recovery of control *Otx* expression pattern in NVPBHG712-treated embryos by simultaneous treatment with a low dose of U0126, the following procedure was adopted. Embryos were treated with 8μM NVPBHG712 from late 16-cell stage and various concentrations of U0126, empirically chosen, around 0.2μM. Following *Otx* smFISH, a few embryos from each experimental condition were verified, firstly, for the efficiency of NVPBHG712-treatment (ectopic *Otx*) and, secondly, for the best 'recovery' dose of U0126. Once the best 'recovery' dose was chosen, all embryos in the three conditions, control, NVPBHG712 alone, and NVPBHG712 plus the chosen dose of U0126, were mounted and scanned by confocal microscopy using the above procedure.

Temporal dynamics of *Otx* transcription

Even though embryos were collected from synchronized batches, hand screened to ensure that all embryos were morphologically at the same stage, we noticed some slight asynchronies when embryos were fixed at 3-minute intervals. Therefore, after processing for *Otx* smFISH, every embryo was verified for its exact developmental stage and rescaled by comparison to a time-lapse movie of mesendoderm cells. During the 32-cell stage, the cell cycle of mesendoderm cells is advanced compared to that of ectoderm cells. During this developmental stage, the mesendoderm nuclei display dynamic changes in terms of their relative positions and their morphology. Embryos were fixed every 3-minutes from the early 32-cell stage, processed for *Otx* smFISH and DAPI counterstained. After confocal acquisition

of *Otx* smFISH signals, embryos were re-photographed from the vegetal side using a wide-field fluorescence microscope for DAPI counterstain. The stage of each embryo was then verified by comparing the DAPI-stained nuclei of the medial A-line and B-line endoderm precursors to the time-lapse movie of the corresponding cells. After every embryo was verified in this way, embryos from one fixation time point were occasionally re-grouped with those in a different fixation time point to match the time-lapse movie based developmental stage. Figure S5A shows images acquired by confocal microscopy of embryos stained with DAPI, and matched to the time-lapse movie to illustrate the position of the endoderm nuclei relative to the nuclei of a6.5 neural precursors at various time points.

Modeling

All modeling was carried out with Matlab software (Mathworks, Massachusetts, USA) and python.

Control of ERK activation by SOS and p120RasGAP

For the modeling results of ERK activation status controlled by both SOS and p120RasGAP (Figures 3D and S4A), the aim of the calculations was to evaluate qualitatively the impact of SOS, p120RasGAP and ephrin-independent transformation of Ras-GTP into Ras-GDP (k_b) on ERK activity (equation (6) in the main text). Thus, standard values of parameters were taken: $K_1 = K_2 = K_{erk} = 0.5$. The concentration of FGF and ephrin and number of receptors were not explicitly considered. A Hill coefficient of 2 was chosen to consider a non-linear activation of the ERK pathway; data with a Hill coefficient of 1 shows similar results and is shown in Figure S4A.

ERK as a function of R or [Fgf] (without Eph signals)

For the model presented in Figure 4C, a Hill coefficient greater than 1 was chosen based on the following reasoning. We fitted best-fit Hill functions to our data measuring the correlation between cell surface contact and dpERK IF signal level (Figures 1E, 2D, and S2A). Best-fit Hill coefficients gave wide or unpredictable confidence intervals (see Table in Figure S2A). Reasons for this variability are likely that the number of cellular configurations available are small, measured ERK activity is variable and cell surface contact measurements are likely made more variable due to the embryo shrinkage we observe with fixation

conditions used for dpERK IF. Despite these caveats, we consistently observed best-fit Hill coefficients greater than 1 in both control (3 independent experiments) and NVP-treated (8 independent experiments). We therefore took our first Hill coefficient of 2.6 for the model presented in Figure 4C. For this model, we imposed n=2.6, K_{DR}=500, basal activity=0.13 and max activity=1. For the graph in Figure 4C (right), we additionally imposed K_d= 100nM. The Hill coefficient of the relationship between ERK and FGF (n_H) is always smaller than the Hill coefficient of the relationship between ERK and R, the number of receptors in contact with FGF-expressing cells (n).

We next wanted to obtain an analytical expression for the Hill coefficient of the relationship between ERK and FGF (n_H) in relation to the Hill coefficient of the relationship between ERK and R (n):

Equation (5) can be rewritten in the form:

$$Erk^* = \frac{1}{1+\left(\frac{K_{DR}}{R}+\frac{K_{DR}K_d}{R.[Fgf]}\right)^n} \qquad (7)$$

To evaluate the Hill coefficient that characterizes the relation between Erk* and [Fgf], we use the fact that it can be calculated in terms of potency as

$$n_H = \frac{\log(81)}{log\left(\frac{[Fgf]_{90}}{[Fgf]_{10}}\right)} \qquad (8)$$

where $[Fgf]_{90}$ and $[Fgf]_{10}$ are the concentrations of FGF needed to produce 90% and 10% of the maximal Erk activity, respectively.

Inverting equation (7) leads to

$$[Fgf] = \frac{\frac{K_{DR}K_d}{R}}{\left(\frac{1}{Erk*}-1\right)^{1/n}-\frac{K_{DR}}{R}} \qquad (9)$$

Letting $[Fgf]$ tend to infinity in equation (7), one gets the maximal normalized Erk activity that can be reached at a given R:

$$Erk^*_{max} = \frac{1}{\left(1+\left(\frac{K_{DR}}{R}\right)^n\right)} \qquad (10)$$

Using equation (9) to calculate $[Fgf]_{90}$, which corresponds to 0.9 Erk^*_{max} and $[Fgf]_{10}$, which corresponds to 0.1 Erk^*_{max}, one obtains the relationship between n_H (Hill coefficient with respect to [Fgf]) and n (Hill coefficient with respect to the number of receptors):

$$n_H = \frac{\log(81)}{log\left(\frac{\left(\frac{1+a^n}{0.1}-1\right)^{1/n}-a}{\left(\frac{1+a^n}{0.9}-1\right)^{1/n}-a}\right)} \qquad (11)$$

where a stands for $\frac{K_{DR}}{R}$.

This demonstrates that whatever the value of *n*, n_H can only be smaller or equal to *n*, as illustrated in Figure S4D. The exact value of *n* depends on *a,* which is the ratio of the K_{DR} (the number of ligand-bound R at half maximum ERK activity) to R (the number of receptors in contact with FGF-expressing cells). The larger the K_{DR}/R the lower the n_H.

ERK as a function of R or [Fgf] (with Eph signals)

In Figure 4D, we investigated if the conclusion that cells have a greater sensitivity to changes in cell surface contact compared to changes in FGF ligand concentration also holds for embryos where ephrin/Eph signals are intact. We combined two of the previous mathematical approaches presented in Figures 3D and 4C.

As before, the evolution equation for the fraction of Ras-GTP (T) is:

$$\frac{dT}{dt} = V_1 \frac{(1-T)}{K_1+1-T} - V_2 \frac{T}{K_2+T} - k_b T \quad \text{where} \quad T = \frac{[Ras-GTP]}{[Ras-GTP]+[Ras-GDP]} \qquad (12)$$

V_1 is the normalized maximal rate of conversion of Ras-GDP to Ras-GTP by SOS, V_2 is the normalized maximal rate of conversion of Ras-GTP to Ras-GDP by p120RasGAP and K_1 and K_2 are the normalized half-saturation constants of SOS and p120RasGAP for their respective substrates, Ras-GDP and Ras-GTP.

To take into account the cell-contact dependent number of ligand-bound FGF receptors, we considered that SOS must be in its active state (=membrane-recruited) (SOS*) to promote the formation of Ras-GTP. The reaction for the activation of SOS:

$$SOS \leftrightarrow SOS^*$$

is modelled with a Hill coefficient n_1 and depends on the number FGF-bound receptors R_B. So, we can re-write the rate V_1 appearing in eq. 1 as:

$$V_1 = V_s \frac{R_B^{n1}}{K_s^{n1}+R_B^{n1}} \qquad (13)$$

with R_B defined as previously:

$$R_B = R \frac{[Fgf]}{[Fgf]+K_d} \qquad (14)$$

where V_s is the maximal rate of SOS activation and K_s is the number of FGF-bound receptors leading to half of the maximal SOS activity. n_1 allows cooperativity in SOS activation to be considered given that two FGF-bound receptors interact to activate SOS (Blum et al., 2019). Similarly, to consider the cell-dependent number of Eph receptors, we considered that

p120RasGAP must be in an active state(=membrane-recruited) (p120RasGAP*) in order to promote the formation of Ras-GDP:

$$p120RasGAP \leftrightarrow p120RasGAP^*$$

The activation of p120RasGAP depends on the number of receptors bound to ephrin (Q_B). Thus, we re-write the transformation rate V_2 appearing in eq. 12 as:

$$V_2 = V_{rg} \frac{Q_B^{n2}}{K_{rg}^{n2}+Q_B^{n2}} \qquad (15)$$

with

$$Q_B = Q \frac{[ephrin]}{[ephrin]+K_e} \qquad (16)$$

where V_{rg} is the maximal rate of p120RasGAP activation, K_{rg} is the number of ephrin-bound Eph receptors leading to half of the maximal p120RasGAP activity. Q is the number of Eph receptors in contact with ephrin, [ephrin] is the ephrin concentration and K_e is the binding constant of ephrin to its receptor.

To account for the fact that the number of Eph receptors exposed to ephrin changes together with the number of FGF receptors exposed to FGF, i.e., that cells that have the highest number of FGF receptors in contact with FGF (R), have also the lowest number of Eph receptors in contact with ephrin (Q), we used the data from Figure 1B. We called the fraction of the cell surface in contact with FGF, S_1, and the fraction of the cell surface in contact with ephrin, S_2. Plotting S_2 as a function of S_1 and fitting the experimental data with a linear function, we obtained the following relation between S_1 and S_2:

$$S_2 = -1.1265*S_1 + 0.9092 \qquad (17)$$

We then linked the surfaces (S_1 and S_2) to the number of receptors potentially available for activation by FGF (R) and ephrin (Q), respectively. Assuming that on the whole cell surface, there are 2000 receptors to FGF and 2000 receptors to ephrin, the number of receptors in contact with FGF (or ephrin) depends on the contact area between the cell and FGF (S_1) or ephrin (S_2): when all the cell surface is in contact with FGF (namely S_1=1) then the number of FGF receptors in contact with FGF will be equal to the total number of FGF receptors present on that cell ($R=R_{tot}$=2000). Thus, we can write $R= R_{tot}S_1$. The same considerations hold for ephrin: $Q= Q_{tot}S_2$. We substituted these last expressions for R and Q into the evolution equation for T (eq. (12)):

$$\frac{dT}{dt} = V_s \frac{{R_B}^{n1}}{K_s^{n1}+R_B^{n1}} \frac{(1-T)}{K_1+1-T} - V_{rg} \frac{Q_B^{n2}}{Q_B^{n2}+K_{rg}^{n2}} \frac{T}{K_2+T} - k_b T \qquad (18)$$

where

$$R_B = R_{tot} S_1 \frac{[Fgf]}{K_d + [Fgf]} \text{ and } Q_B = Q_{tot} S_2 \frac{[ephrin]}{K_e + [ephrin]} \qquad (19, 20)$$

Next, we solved the equation for T at equilibrium, obtaining T as a function of [Fgf] or as a function of S_1. This gives us the relation between the fraction of Ras-GTP and [Fgf] or S_1. It is important to remember that S_2 changes at the same time as S_1 because eq. (17) is always satisfied. We then computed the fraction of active Erk (Erk*) assuming that the relation between Erk* and T is the same as before (eq. (2) in the main text), i.e.:

$$Erk^* = \frac{Erk}{Erk_{\max}} = \frac{T^2}{T^2 + K_{erk}^2}$$

We computed Erk* as a function of [Fgf] and as a function of S_1. For both curves, we evaluated the Hill coefficient using the definition:

$n_{HF} = \frac{log(81)}{log\left(\frac{[Fgf]_{90}}{[Fgf]_{10}}\right)}$ for the Hill coefficient of Erk* as a function of FGF concentration

or $n_{HS} = \frac{log(81)}{log\left(\frac{(S_1)_{90}}{(S_1)_{10}}\right)}$ for the Hill coefficient of Erk* as a function of S1

The standard values of the parameters used in the calculation are V_s= 1, K_{rg}= 500, K_e= 500, K_d= 500, K_1= 0.5, K_2= 0.5, V_{rg}= 0.25, K_s= 500, k_b= 0.2, R_{tot}= 2000, Q_{tot}= 2000, n1=1, n2=1. Similar results were obtained with n1=2, n2=2; n1=2, n2=1 and n1=1, n2=2 (not shown).

Competitive regulation of Otx expression

To test the concept that competitive regulation of *Otx* expression by an activator and a repressor (hereafter called inhibitor), which are both controlled by ERK activity, would increase the sensitivity of the *Otx* activation response to ERK, we used a phenomenological model schematized in Figure 6C. dpERK controls *Otx* expression by the stimulation of an activator (A; e.g. ETS, in blue) and by the suppression of an inhibitor (I; e.g. ERF, in red). The evolution equations, describing the phosphorylation and dephosphorylation of ETS (A: eq. 21) and ERF (I: eq. 22) are:

$$\frac{dA_p}{dt} = k_{MM3} E \frac{(1 - A_p)}{K_{MM3} + 1 - A_p} - v_{MM4} \frac{A_p}{K_{MM4} + A_p} \quad (21) \qquad A \underset{v_{MM4}}{\overset{k_{MM3}}{\rightleftharpoons}} A_p$$

$$\frac{dI}{dt} = v_{MM2} \frac{(1 - I)}{K_{MM2} + 1 - I} - k_{MM1} E \frac{I}{K_{MM1} + I} \quad (22) \qquad I \underset{v_{MM2}}{\overset{k_{MM1}}{\rightleftharpoons}} I_p$$

Where Ap represents the fraction of active, phosphorylated activator; 1- A_p the fraction of inactive, unphosphorylated activator; I the fraction of active, unphosphorylated inhibitor and 1- I the fraction of inactive, phosphorylated inhibitor. For the two phosphorylation reactions, the rate constants k_{MM3} and k_{MM1} of A and I phosphorylation are multiplied by the concentration of phosphorylated ERK (E). v_{MM4} and v_{MM2} are the maximal rates at which A_p and I_p are dephosphorylated. K_{MM3} and K_{MM1} are Michaelis-Menten constants for the phosphorylation of A and I, respectively, and K_{MM2} and K_{MM4} are Michaelis-Menten constants for the dephosphorylation of I_p and A_p, respectively. K_{MM3} and K_{MM4} are normalized with respect to the total activator concentrations, while K_{MM2} and K_{MM1} are normalized with respect to the total inhibitor concentrations.

Phosphorylated ETS (A_p) activates the expression of *Otx*, while unphosphorylated ERF (I) inhibits *Otx* expression. Thus, we modelled *Otx* expression with the following evolution equation:

$$\frac{dO}{dt} = v_b + v_o \frac{A_p}{K_a\left(1 + \frac{I}{K_i}\right) + A_p} - k\,O \quad (23)$$

where v_b is the basal *Otx* expression rate, v_o+v_b is the maximal *Otx* expression rate and k is the degradation rate for *Otx*. K_a is the half saturation constant for the activator A_p while K_i is dissociation constant for the inhibitor. In equation (23), it is considered that ERF (I) is a competitive inhibitor of ETS (A). Thus, there is an effective half-saturation constant that depends on the concentration of I, which is equal to $K_a\left(1 + \frac{I}{K_i}\right)$. Thus, when I is large, this effective constant is much larger than K_a and, when I is small, this effective constant approaches K_a. In order to obtain *Otx* as a function of E, we solved equations (21)-(23) at equilibrium. Figure 6D (left) shows the concentration of the inhibitor (red line) and of the activator (green line) as a function of E obtained solving equations (21) and (22), while Figure 6D (right) shows the curves Otx(E) in the presence (blue line) and in the absence (orange line; I=0) of the inhibitor, obtained using eq. (23). Standard parameters used are: k_{MM3}= 0.1, k_{MM1}= 0.1, K_{MM3} = K_{MM4} = 0.2, K_{MM1} = K_{MM2} = 0.8, v_{MM2} = v_{MM4} = 1, K_a = 0.1, K_i = 0.1, v_b = 0.01, v_o = 1, k = 0.2. Hill curves are fitted to the lower half of the curve (up to approximately *Otx*=2.5). Hill coefficients obtained following parameter changes are shown in Figure S7F.

QUANTIFICATION AND STATISTICAL ANALYSIS

Embryo reconstruction with Amira software

For the *PH-GFP* injected embryos stained with α-GFP IF, embryo reconstruction and surface area calculations were carried out with Amira software (Thermo Fisher Scientific, Massachusetts, USA). Briefly, the stack was opened with the software and a "Membrane Enhancement Filter" was applied to enhance the membrane signal and suppress any cytoplasmic background. From this cleaned stack, the outer surface of the embryo was segmented with the "magic wand" tool and assigned to an "Exterior" object. Then a semi-automatic process was carried out in order to obtain a precise segmentation. Each cell was tagged manually with the "brush" tool in each dimension (XY, XZ and YZ) and assigned to an object with the name of the corresponding cell. A watershed segmentation was applied, generating automatically 32 objects corresponding to the total 32 cells of the embryo. At this step and only if necessary, some cells were corrected by hand with the "brush" tool. A smoothing pipeline (smooth labels and remove island) was then applied in order to remove any isolated pixels. Finally, the 3D surface was generated by the software and surface data were computed and extracted as an Excel file.

For the Phalloidin-stained embryos shown in Figure 2B, the processes of embryo reconstruction and surface data calculation were described previously (Robin et al., 2011b) and conducted with slight modifications. We used 3 different software packages: Avizo software (Thermo Scientific), 3DStudioMax (3dsMax, Autodesk) and 3D Virtual Embryo (3DVE, ANISEED (Tassy et al., 2010)). Briefly, the stack was opened with Avizo software. The outer surface of the embryo was segmented with the "magic wand" tool and assigned to an "Exterior" object. Then a manual segmentation of each cell was carried out with a graphic tablet (Wacom, Kazo, Japan), by delimiting cells manually one by one. At the beginning of a cell, the contour was drawn with the "brush" tool in the xy dimension and then the contour was filled. 2 or 3 slices after, the same process was done until reaching the end of the cell. Intermediate slices were then interpolated and included in the selection. The selection corresponding to the cell was assigned to an object with the corresponding name. This procedure was repeated for the total 32 cells of the embryo. A smoothing pipeline (smooth labels and remove island) was applied in order to remove any isolated pixels. The 3D surfaces were generated by Avizo software and exported in a format compatible with 3dsMax software (VRML). With this software, on each cell, a process of normalization of the vertex was done in order to unify all the surfaces and another pipeline of smoothing was

applied. Then, the virtual embryo with smoothed cell surfaces was exported in a format compatible with 3DVE software (Wavefront) (Robin et al., 2011b). Finally, surfaces and the cell-cell contact surfaces were calculated with 3DVE. The semi-automated reconstruction using Amira and PH-GFP labelled embryos described first was far superior in ease and rapidity and was used for all other reconstructions.

dpERK IF- and GFP IF- stained embryos

Imaris software (Oxford instruments, Abingdon, UK) was used for quantification of dpERK IF signals. H3 channels were used to segment nuclei, enabling automated measurements of the mean pixel intensity of each nucleus in the dpERK channel. In the FGFR-MO plus FGFR mRNA 'rescue' experiment (Figure 4B), we used the FGFR-MO-only injected halves to select for efficiency of *FGFR* knockdown. We disregarded all embryos that had more than 30% difference in mean pixel intensities of dpERK IF signals between a6.5 and a6.8 on the FGFR-MO-only injected half. Following this stringent selection criteria, no significant difference was observed among any pair of a-line cells from the FGFR-MO injected side, in paired t-tests. For the dpERK IF images shown in Figures 1C and 4B we applied a dust and scratches filter (Adobe Photoshop).

Quantification of GFP IF signals on *FGFR-Venus* injected embryos was performed on maximum intensity projections of selected two consecutive planes of 0.75μm thickness. Using Fiji software (Schindelin et al., 2012), a line of 5 pixel width (0.8μm) was drawn along the three distinct regions of membranes indicated in Figure S4B to obtain their mean signal intensities.

ERK-KTR

Time-lapse movies were normalized to t=0 at the point of nuclear envelope breakdown (NEBD) of A6.4 cells. t= 4-8 corresponds to 'late 32-cell stage', when vegetal cells undergo de-compaction and embryos become flattened in shape. Image quantification was carried out with ImageJ software (Rueden et al., 2017). First, the background was subtracted from the ERK-KTR hyperstack using a custom-made Java plugin. A ROI was set on the largest disc corresponding to each nucleus of the a-line ectoderm cells in each time point using the NLS-Tomato hyperstack. Then, these ROIs were applied on the ERK-KTR hyperstack and a mean

intensity measurement was obtained for each nucleus. On the z-slice with the nucleus largest disc, a mean intensity measurement of the ROI defined manually by tracing the contour of the corresponding cell was also obtained for each a-line ectoderm cell at each time point. This "cytoplasmic" ERK-KTR mean intensity was divided by the nuclear ERK-KTR mean intensity to obtain cytoplasmic/nuclear ratios. To normalize between embryos, the cytoplasmic/nuclear ratio of each cell within an embryo was normalized by dividing by the mean a6.8 cytoplasmic/nuclear ratio obtained across all time points. This normalized value is indicated as 'C/N' in the text.

In embryos injected with *dnFGFR* mRNA in one cell at the 2-cell stage, the ERK-KTR signal at the 32-cell stage gradually increased in all cells on both sides, as well as in embryos treated with U0126 (Figures S1G and S1H). This gradual increase over time is therefore not due to FGF/MEK signals, but most likely due to continuous translation of the biosensor over time. In our analysis with anti-dpERK IF, we showed that levels of ERK activity in a6.8 were similar to unstimulated (FGF/MEK inhibited) levels (Figure 2A and S1D). In addition, ERK-KTR C/N ratios of a6.8 on the control sides grouped with cells on the *dnFGFR*-injected sides (Figure S1G, black line on 'dnFGFR side' graph). For our temporal analysis, therefore, for each embryo half, we normalized each C/N ratio to the C/N ratio of the corresponding a6.8 cell at each time point to give "C/N normalized to a6.8".

Western blot

Images acquired with Fusion were quantified with Fiji software after background subtraction (rolling ball 50 pixels) (Schindelin et al., 2012). Each dpERK value was normalized by the loading control PKCζ value and data between blots was normalized by dividing each dpERK/PKCζ ratio with the ratio of the whole embryo standard (3 or 4 whole embryos) loaded onto every gel in the linear range test. Quantified points outside of the linear range (either dpERK or PKCζ), those with signal levels considerably higher than other points (spurious points) or those obscured by particles or bubbles during antibody incubation were removed from the analysis. For the graph shown in Figure 3B, in total 8 out of 238 points were removed.

smFISH

smFISH spots were counted in the segmented nuclei of high resolution images with Imaris software (Oxford Instruments). For all smFISH spot counts, values of 0 were changed to 0.1 so graphs could be presented with a logarithmic scale. In order to test whether this smFISH method allows us to detect *Otx* transcripts in a semi-quantitative manner, we injected synthetic *Otx* mRNA (0.1, 0.2, 0.4ng/μl) into single a4.2 cells of 8-cell stage embryos and analyzed them with *Otx* smFISH at 16-cell stage before endogenous *Otx* expression started. We found that this method allows us to detect incremental two-fold increases of transcript levels in *Ciona* embryos (not shown). Furthermore, histograms of spot signal intensity show a single peak, which is consistent with one spot representing one transcript.

Graphs and statistical tests

Graphical representations in all Figures (except for modeling) and statistical tests (except Hartigan's diptest) were conducted with Prism 8-GraphPad software (California, USA). The statistical tests used is indicated in each figure legend.

For Hatigan's diptest of unimodality, R Studio (https://rstudio.com) was used, with the diptest addin (https://cran.r-project.org/web/packages/diptest/index.html).

REFERENCES

Ahmed, S., Grant, K.G., Edwards, L.E., Rahman, A., Cirit, M., Goshe, M.B., and Haugh, J.M. (2014). Data-driven modeling reconciles kinetics of ERK phosphorylation, localization, and activity states. Mol. Syst. Biol. *10*, 718.

Albeck, J.G., Mills, G.B., and Brugge, J.S. (2013). Frequency-modulated pulses of ERK activity transmit quantitative proliferation signals. Mol. Cell *49*, 249–261.

Aoki, K., Yamada, M., Kunida, K., Yasuda, S., and Matsuda, M. (2011). Processive phosphorylation of ERK MAP kinase in mammalian cells. Proc. Natl. Acad. Sci. *108*, 12675–12680.

Aoki, K., Kumagai, Y., Sakurai, A., Komatsu, N., Fujita, Y., Shionyu, C., and Matsuda, M. (2013). Stochastic ERK Activation Induced by Noise and Cell-to-Cell Propagation Regulates Cell Density-Dependent Proliferation. Mol. Cell *52*, 529–540.

Azaripour, A., Lagerweij, T., Scharfbillig, C., Jadczak, A.E., Willershausen, B., and Van Noorden, C.J.F. (2016). A survey of clearing techniques for 3D imaging of tissues with special reference to connective tissue. Prog. Histochem. Cytochem. *51*, 9–23.

Bertrand, V., Hudson, C., Caillol, D., Popovici, C., and Lemaire, P. (2003). Neural tissue in ascidian embryos is induced by FGF9/16/20, acting via a combination of maternal GATA and Ets transcription factors. Cell *115*, 615–627.

Blum, Y., Mikelson, J., Dobrzyński, M., Ryu, H., Jacques, M., Jeon, N.L., Khammash, M., and Pertz, O. (2019). Temporal perturbation of ERK dynamics reveals network architecture of FGF2/MAPK signaling. Mol. Syst. Biol. *15*.

van Boxtel, A.L., Economou, A.D., Heliot, C., and Hill, C.S. (2018). Long-Range Signaling Activation and Local Inhibition Separate the Mesoderm and Endoderm Lineages. Dev. Cell *44*, 179-191.e5.

Brozovic, M., Dantec, C., Dardaillon, J., Dauga, D., Faure, E., Gineste, M., Louis, A., Naville, M., Nitta, K.R., Piette, J., et al. (2018). ANISEED 2017: extending the integrated ascidian database to the exploration and evolutionary comparison of genome-scale datasets. Nucleic Acids Res. *46*, D718–D725.

Carroll, M., Levasseur, M., Wood, C., Whitaker, M., Jones, K., and McDougall, A. (2003). Exploring the mechanism of action of the sperm-triggered calcium-wave pacemaker in ascidian zygotes. J. Cell Sci. *116*, 4997–5004.

Conklin, E.G. (1905). The organisation and cell lineage of the ascidian egg. J Acad Natl Sci Phila. 1–119.

Coppey, M., Boettiger, A.N., Berezhkovskii, A.M., and Shvartsman, S.Y. (2008). Nuclear trapping shapes the terminal gradient in the Drosophila embryo. Curr. Biol. CB *18*, 915–919.

Cota, C.D., and Davidson, B. (2015). Mitotic Membrane Turnover Coordinates Differential Induction of the Heart Progenitor Lineage. Dev. Cell *34*, 505–519.

de la Cova, C., Townley, R., Regot, S., and Greenwald, I. (2017). A Real-Time Biosensor for ERK Activity Reveals Signaling Dynamics during C. elegans Cell Fate Specification. Dev. Cell *42*, 542-553.e4.

Delsuc, F., Philippe, H., Tsagkogeorga, G., Simion, P., Tilak, M.-K., Turon, X., López-Legentil, S., Piette, J., Lemaire, P., and Douzery, E.J.P. (2018). A phylogenomic framework and timescale for comparative studies of tunicates. BMC Biol. *16*, 39.

Dent, J.A., Polson, A.G., and Klymkowsky, M.W. (1989). A whole-mount immunocytochemical analysis of the expression of the intermediate filament protein vimentin in Xenopus. Development *105*, 61.

Dorey, K., and Amaya, E. (2010). FGF signalling: diverse roles during early vertebrate embryogenesis. Development *137*, 3731–3742.

Ebisuya, M., Kondoh, K, and Nishida, E. (2005). The duration, magnitude and compartmentalization of ERK MAP kinase activity: mechanisms for providing signaling specificity. J. Cell Sci. *118*, 2997–3002.

Engl, W., Arasi, B., Yap, L.L., Thiery, J.P., and Viasnoff, V. (2014). Actin dynamics modulate mechanosensitive immobilization of E-cadherin at adherens junctions. Nat. Cell Biol. *16*, 584–591.

Esposito, R., Yasuo, H., Sirour, C., Palladino, A., Spagnuolo, A., and Hudson, C. (2017). Patterning of brain precursors in ascidian embryos. Development *144*, 258–264.

Farley, E.K., Olson, K.M., Zhang, W., Brandt, A.J., Rokhsar, D.S., and Levine, M.S. (2015). Suboptimization of developmental enhancers. Science *350*, 325–328.

Ferrell Jr., J.E., and Machleder, E.M. (1998). The Biochemical Basis of an All-or-None Cell Fate Switch in Xenopus Oocytes. Science *280*, 895–898.

Fiuza, U.-M., Negishi, T., Rouan, A., Yasuo, H., and Lemaire, P. (2020). A Nodal/Eph signalling relay drives the transition from apical constriction to apico-basal shortening in ascidian endoderm invagination. Dev. Camb. Engl. *in press*.

Francavilla, C., Rigbolt, K.T.G., Emdal, K.B., Carraro, G., Vernet, E., Bekker-Jensen, D.B., Streicher, W., Wikström, M., Sundström, M., Bellusci, S., et al. (2013). Functional Proteomics Defines the Molecular Switch Underlying FGF Receptor Trafficking and Cellular Outputs. Mol. Cell *51*, 707–722.

Gibson, D.G., Young, L., Chuang, R.-Y., Venter, J.C., Hutchison, C.A., and Smith, H.O. (2009). Enzymatic assembly of DNA molecules up to several hundred kilobases. Nat. Methods *6*, 343–345.

Gilchrist, M.J., Sobral, D., Khoueiry, P., Daian, F., Laporte, B., Patrushev, I., Matsumoto, J., Dewar, K., Hastings, K.E.M., Satou, Y., et al. (2015). A pipeline for the systematic identification of non-redundant full-ORF cDNAs for polymorphic and evolutionary divergent genomes: Application to the ascidian Ciona intestinalis. Dev. Biol. *404*, 149–163.

Guignard, L., Fiúza, U.-M., Leggio, B., Laussu, J., Faure, E., Michelin, G., Biasuz, K., Hufnagel, L., Malandain, G., Godin, C., et al. (2020). Contact area–dependent cell communication and the morphological invariance of ascidian embryogenesis. Science *369*, eaar5663.

Haupaix, N., Stolfi, A., Sirour, C., Picco, V., Levine, M., Christiaen, L., and Yasuo, H. (2013). p120RasGAP mediates ephrin/Eph-dependent attenuation of FGF/ERK signals during cell fate specification in ascidian embryos. Dev. Camb. Engl. *140*, 4347–4352.

Huang, C.Y., and Ferrell, J.E. (1996). Ultrasensitivity in the mitogen-activated protein kinase cascade. Proc. Natl. Acad. Sci. U. S. A. *93*, 10078–10083.

Hudson, C. (2016). The central nervous system of ascidian larvae. Wiley Interdiscip. Rev. Dev. Biol. *doi: 10.1002/wdev.239*.

Hudson, C. (2020). A Simple Method to Identify Ascidian Brain Lineage Cells at Neural Plate Stages Following In Situ Hybridization. In Brain Development, S.G. Sprecher, ed. (New York, NY: Springer New York), pp. 325–345.

Hudson, C., and Lemaire, P. (2001). Induction of anterior neural fates in the ascidian Ciona intestinalis. Mech. Dev. *100*, 189–203.

Hudson, C., Darras, S., Caillol, D., Yasuo, H., and Lemaire, P. (2003). A conserved role for the MEK signalling pathway in neural tissue specification and posteriorisation in the invertebrate chordate, the ascidian Ciona intestinalis. Dev. Camb. Engl. *130*, 147–159.

Hudson, C., Lotito, S., and Yasuo, H. (2007). Sequential and combinatorial inputs from Nodal, Delta2/Notch and FGF/MEK/ERK signalling pathways establish a grid-like organisation of distinct cell identities in the ascidian neural plate. Dev. Camb. Engl. *134*, 3527–3537.

Hudson, C., Sirour, C., and Yasuo, H. (2016). Co-expression of Foxa.a, Foxd and Fgf9/16/20 defines a transient mesendoderm regulatory state in ascidian embryos. ELife *5*.

Inazawa, T., Okamura, Y., and Takahashi, K. (1998). Basic fibroblast growth factor induction of neuronal ion channel expression in ascidian ectodermal blastomeres. J. Physiol. *511*, 347–359.

Johnson, H.E., and Toettcher, J.E. (2019). Signaling Dynamics Control Cell Fate in the Early Drosophila Embryo. Dev. Cell *48*, 361-370.e3.

Ke, M.-T., Fujimoto, S., and Imai, T. (2013). SeeDB: a simple and morphology-preserving optical clearing agent for neuronal circuit reconstruction. Nat. Neurosci. *16*, 1154–1161.

Kim, G.J., and Nishida, H. (2001). Role of the FGF and MEK signaling pathway in the ascidian embryo. Dev. Growth Differ. *43*, 521–533.

Klein, R. (2012). Eph/ephrin signalling during development. Development *139*, 4105–4109.

Le Gallic, L., Sgouras, D., Beal, G., and Mavrothalassitis, G. (1999). Transcriptional repressor ERF is a Ras/mitogen-activated protein kinase target that regulates cellular proliferation. Mol. Cell. Biol. *19*, 4121–4133.

Le Gallic, L., Virgilio, L., Cohen, P., Biteau, B., and Mavrothalassitis, G. (2004). ERF nuclear shuttling, a continuous monitor of Erk activity that links it to cell cycle progression. Mol. Cell. Biol. *24*, 1206–1218.

Lemaire, P., Garrett, N., and Gurdon, J.B. (1995). Expression cloning of Siamois, a xenopus homeobox gene expressed in dorsal-vegetal cells of blastulae and able to induce a complete secondary axis. Cell *81*, 85–94.

Lemmon, M.A., and Schlessinger, J. (2010). Cell Signaling by Receptor Tyrosine Kinases. Cell *141*, 1117–1134.

Lim, B., Samper, N., Lu, H., Rushlow, C., Jiménez, G., and Shvartsman, S.Y. (2013). Kinetics of gene derepression by ERK signaling. Proc. Natl. Acad. Sci. U. S. A. *110*, 10330–10335.

Lim, B., Dsilva, C.J., Levario, T.J., Lu, H., Schüpbach, T., Kevrekidis, I.G., and Shvartsman, S.Y. (2015). Dynamics of Inductive ERK Signaling in the Drosophila Embryo. Curr. Biol. CB *25*, 1784–1790.

MacKeigan, J.P., Murphy, L.O., Dimitri, C.A., and Blenis, J. (2005). Graded Mitogen-Activated Protein Kinase Activity Precedes Switch-Like c-Fos Induction in Mammalian Cells. Mol. Cell. Biol. *25*, 4676–4682.

Markevich, N.I., Hoek, J.B., and Kholodenko, B.N. (2004). Signaling switches and bistability arising from multisite phosphorylation in protein kinase cascades. J. Cell Biol. *164*, 353–359.

Melen, G.J., Levy, S., Barkai, N., and Shilo, B. (2005). Threshold responses to morphogen gradients by zero-order ultrasensitivity. Mol. Syst. Biol. *1*.

Miyazaki, Y., Nishida, H., and Kumano, G. (2007). Brain induction in ascidian embryos is dependent on juxtaposition of FGF9/16/20-producing and -receiving cells. Dev. Genes Evol. *217*, 177–188.

Nishida, H. (1987). Cell lineage analysis in ascidian embryos by intracellular injection of a tracer enzyme. III. Up to the tissue restricted stage. Dev. Biol. *121*, 526–541.

Nishida, H. (2003). Spatio-temporal pattern of MAP kinase activation in embryos of the ascidian Halocynthia roretzi. Dev. Growth Differ. *45*, 27–37.

Nunns, H., and Goentoro, L. (2018). Signaling pathways as linear transmitters. ELife *7*, e33617.

Ohta, N., and Satou, Y. (2013). Multiple signaling pathways coordinate to induce a threshold response in a chordate embryo. PLoS Genet. *9*, e1003818.

Ohta, N., Waki, K., Mochizuki, A., and Satou, Y. (2015). A Boolean Function for Neural Induction Reveals a Critical Role of Direct Intercellular Interactions in Patterning the Ectoderm of the Ascidian Embryo. PLoS Comput. Biol. *11*, e1004687.

Ornitz, D.M., and Itoh, N. (2015). The Fibroblast Growth Factor signaling pathway. Wiley Interdiscip. Rev. Dev. Biol. *4*, 215–266.

Perrett, R.M., Fowkes, R.C., Caunt, C.J., Tsaneva-Atanasova, K., Bowsher, C.G., and McArdle, C.A. (2013). Signaling to Extracellular Signal-regulated Kinase from ErbB1 Kinase and Protein Kinase C: FEEDBACK, HETEROGENEITY, AND GATING. J. Biol. Chem. *288*, 21001–21014.

Picco, V., Hudson, C., and Yasuo, H. (2007). Ephrin-Eph signalling drives the asymmetric division of notochord/neural precursors in Ciona embryos. Dev. Camb. Engl. *134*, 1491–1497.

Pokrass, M.J., Ryan, K.A., Xin, T., Pielstick, B., Timp, W., Greco, V., and Regot, S. (2020). Cell-Cycle-Dependent ERK Signaling Dynamics Direct Fate Specification in the Mammalian Preimplantation Embryo. Dev. Cell *55*, 328-340.e5.

Prodon, F., Chenevert, J., Hébras, C., Dumollard, R., Faure, E., Gonzalez-Garcia, J., Nishida, H., Sardet, C., and McDougall, A. (2010). Dual mechanism controls asymmetric spindle position in ascidian germ cell precursors. Dev. Camb. Engl. *137*, 2011–2021.

Regot, S., Hughey, J.J., Bajar, B.T., Carrasco, S., and Covert, M.W. (2014). High-Sensitivity Measurements of Multiple Kinase Activities in Live Single Cells. Cell *157*, 1724–1734.

Robin, F.B., Dauga, D., Tassy, O., Sobral, D., Daian, F., and Lemaire, P. (2011a). Imaging of Fixed Ciona Embryos for Creating 3D Digital Replicas. Cold Spring Harb. Protoc. *2011*, pdb.prot065854-pdb.prot065854.

Robin, F.B., Dauga, D., Tassy, O., Sobral, D., Daian, F., and Lemaire, P. (2011b). Creating 3D Digital Replicas of Ascidian Embryos from Stacks of Confocal Images. Cold Spring Harb. Protoc. *2011*, pdb.prot065862-pdb.prot065862.

Rothbächer, U., Bertrand, V., Lamy, C., and Lemaire, P. (2007). A combinatorial code of maternal GATA, Ets and beta-catenin-TCF transcription factors specifies and patterns the early ascidian ectoderm. Dev. Camb. Engl. *134*, 4023–4032.

Roure, A., Rothbächer, U., Robin, F., Kalmar, E., Ferone, G., Lamy, C., Missero, C., Mueller, F., and Lemaire, P. (2007). A multicassette Gateway vector set for high throughput and comparative analyses in ciona and vertebrate embryos. PloS One *2*, e916.

Rueden, C.T., Schindelin, J., Hiner, M.C., DeZonia, B.E., Walter, A.E., Arena, E.T., and Eliceiri, K.W. (2017). ImageJ2: ImageJ for the next generation of scientific image data. BMC Bioinformatics *18*, 529.

Ryu, H., Chung, M., Dobrzyński, M., Fey, D., Blum, Y., Lee, S.S., Peter, M., Kholodenko, B.N., Jeon, N.L., and Pertz, O. (2015). Frequency modulation of ERK activation dynamics rewires cell fate. Mol. Syst. Biol. *11*, 838.

Santos, S.D.M., Verveer, P.J., and Bastiaens, P.I.H. (2007). Growth factor-induced MAPK network topology shapes Erk response determining PC-12 cell fate. Nat. Cell Biol. *9*, 324–330.

Sardet, C., McDougall, A., Yasuo, H., Chenevert, J., Pruliere, G., Dumollard, R., Hudson, C., Hebras, C., Le Nguyen, N., and Paix, A. (2011). Embryological methods in ascidians: the Villefranche-sur-Mer protocols. Methods Mol. Biol. Clifton NJ *770*, 365–400.

Satou, Y., Sasakura, Y., Yamada, L., Imai, K.S., Satoh, N., and Degnan, B. (2003). A genomewide survey of developmentally relevant genes in Ciona intestinalis: V. Genes for receptor tyrosine kinase pathway and Notch signaling pathway. Dev. Genes Evol. *213*, 254–263.

Satou, Y., Kawashima, T., Shoguchi, E., Nakayama, A., and Satoh, N. (2005). An integrated database of the ascidian, Ciona intestinalis: towards functional genomics. Zoolog. Sci. *22*, 837–843.

Satou, Y., Mineta, K., Ogasawara, M., Sasakura, Y., Shoguchi, E., Ueno, K., Yamada, L., Matsumoto, J., Wasserscheid, J., Dewar, K., et al. (2008). Improved genome assembly and evidence-based global gene model set for the chordate Ciona intestinalis: new insight into intron and operon populations. Genome Biol. *9*, R152.

Satou, Y., Nakamura, R., Yu, D., Yoshida, R., Hamada, M., Fujie, M., Hisata, K., Takeda, H., and Satoh, N. (2019). A Nearly Complete Genome of Ciona intestinalis Type A (C. robusta) Reveals the Contribution of Inversion to Chromosomal Evolution in the Genus Ciona. Genome Biol. Evol. *11*, 3144–3157.

Schindelin, J., Arganda-Carreras, I., Frise, E., Kaynig, V., Longair, M., Pietzsch, T., Preibisch, S., Rueden, C., Saalfeld, S., Schmid, B., et al. (2012). Fiji: an open-source platform for biological-image analysis. Nat. Methods *9*, 676–682.

Shankaran, H., Ippolito, D.L., Chrisler, W.B., Resat, H., Bollinger, N., Opresko, L.K., and Wiley, H.S. (2009). Rapid and sustained nuclear–cytoplasmic ERK oscillations induced by epidermal growth factor. Mol. Syst. Biol. *5*, 332.

Shindo, Y., Iwamoto, K., Mouri, K., Hibino, K., Tomita, M., Kosako, H., Sako, Y., and Takahashi, K. (2016). Conversion of graded phosphorylation into switch-like nuclear translocation via autoregulatory mechanisms in ERK signalling. Nat. Commun. *7*, 10485.

Simon, C.S., Rahman, S., Raina, D., Schröter, C., and Hadjantonakis, A.-K. (2020). Live Visualization of ERK Activity in the Mouse Blastocyst Reveals Lineage-Specific Signaling Dynamics. Dev. Cell *55*, 341-353.e5.

Stolfi, A., Wagner, E., Taliaferro, J.M., Chou, S., and Levine, M. (2011). Neural tube patterning by Ephrin, FGF and Notch signaling relays. Dev. Camb. Engl. *138*, 5429–5439.

Tassy, O., Daian, F., Hudson, C., Bertrand, V., and Lemaire, P. (2006). A quantitative approach to the study of cell shapes and interactions during early chordate embryogenesis. Curr. Biol. CB *16*, 345–358.

Tassy, O., Dauga, D., Daian, F., Sobral, D., Robin, F., Khoueiry, P., Salgado, D., Fox, V., Caillol, D., Schiappa, R., et al. (2010). The ANISEED database: digital representation, formalization, and elucidation of a chordate developmental program. Genome Res. *20*, 1459–1468.

Turner, N., and Grose, R. (2010). Fibroblast growth factor signalling: from development to cancer. Nat. Rev. Cancer *10*, 116–129.

Yagi, K., Satou, Y., Mazet, F., Shimeld, S.M., Degnan, B., Rokhsar, D., Levine, M., Kohara, Y., and Satoh, N. (2003). A genomewide survey of developmentally relevant genes in Ciona intestinalis. III. Genes for Fox, ETS, nuclear receptors and NFkappaB. Dev. Genes Evol. *213*, 235–244.

Yasuo, H., and McDougall, A. (2018). Practical Guide for Ascidian Microinjection: Phallusia mammillata. In Transgenic Ascidians, Y. Sasakura, ed. (Singapore: Springer Singapore), pp. 15–24.

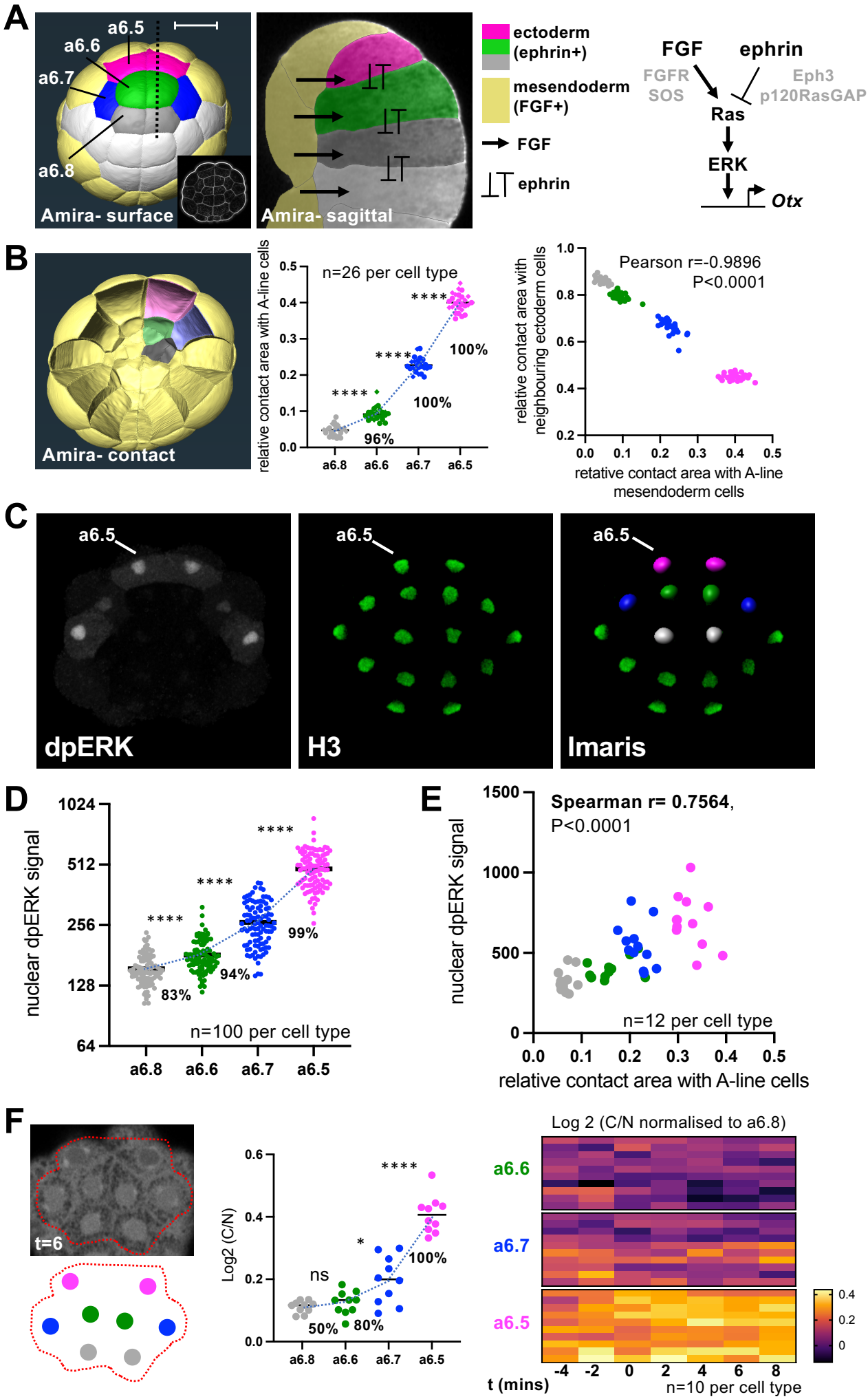
A
a6.5
a6.6
a6.7
a6.8
Amira- surface
Amira- sagittal
ectoderm
(ephrin+)
mesendoderm
(FGF+)
FGF
ephrin
FGF
ephrin
FGFR
SOS
Eph3
p120RasGAP
Ras
ERK
Otx
B
Amira- contact
n=26 per cell type
relative contact area with A-line cells
****
100%
96%
a6.8
a6.6
a6.7
a6.5
Pearson r=-0.9896
P<0.0001
relative contact area with neighbouring ectoderm cells
retative contact area with A-line mesendoderm cells
C
dpERK
H3
Imaris
D
nuclear dpERK signal
n=100 per cell type
83%
94%
99%
E
Spearman r= 0.7564,
P<0.0001
nuclear dpERK signal
n=12 per cell type
relative contact area with A-line cells
F
t=6
Log2 (C/N)
ns
*
50%
80%
Log 2 (C/N normalised to a6.8)
t (mins)
n=10 per cell type

Figure 1

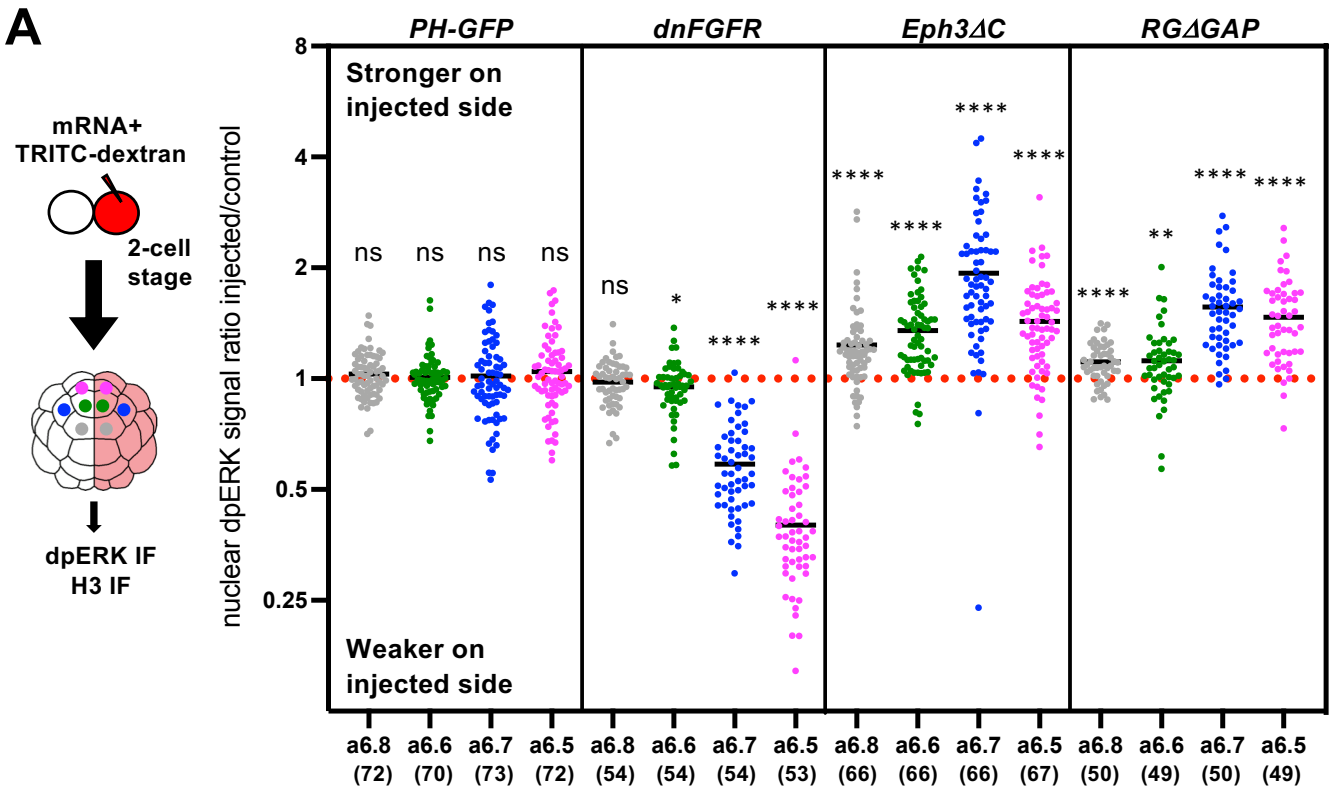
A
mRNA+
TRITC-dextran
2-cell
stage
dpERK IF
H3 IF
PH-GFP
dnFGFR
Eph3ΔC
RGΔGAP
Stronger on
injected side
Weaker on
injected side
nuclear dpERK signal ratio injected/control
8
4
2
1
0.5
0.25
ns
*
**
****
a6.8 (72)
a6.6 (70)
a6.7 (73)
a6.5 (72)
a6.8 (54)
a6.6 (54)
a6.7 (54)
a6.5 (53)
a6.8 (66)
a6.6 (66)
a6.7 (66)
a6.5 (67)
a6.8 (50)
a6.6 (49)
a6.7 (50)
a6.5 (49)

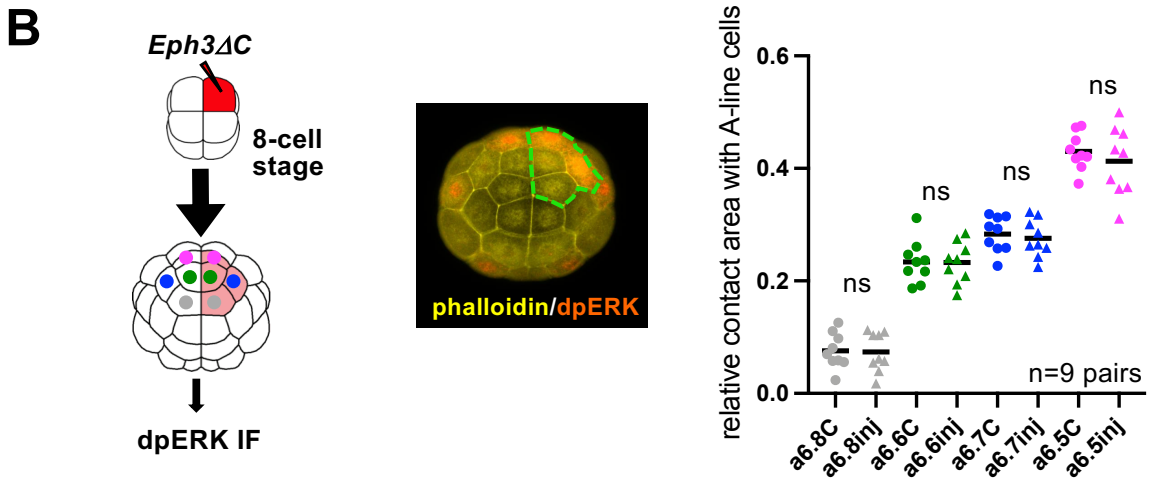
B
Eph3ΔC
8-cell
stage
dpERK IF
phalloidin/dpERK
relative contact area with A-line cells
0.6
0.4
0.2
0.0
ns
n=9 pairs
a6.8C
a6.8inj
a6.6C
a6.6inj
a6.7C
a6.7inj
a6.5C
a6.5inj

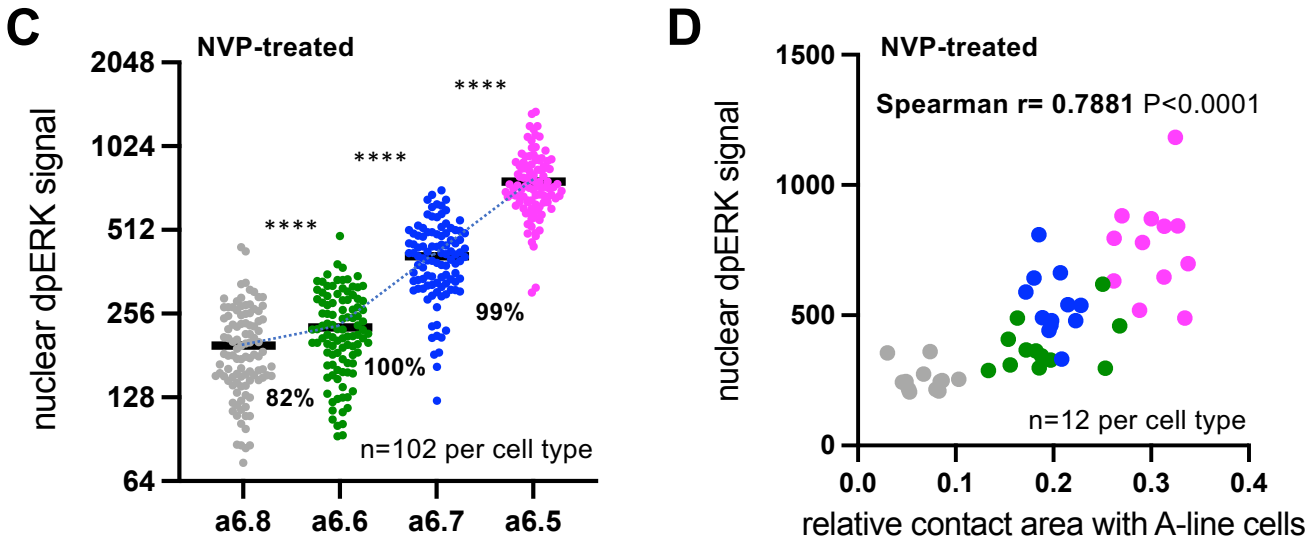
C
NVP-treated
nuclear dpERK signal
2048
1024
512
256
128
64
****
82%
100%
99%
n=102 per cell type
a6.8
a6.6
a6.7
a6.5
D
NVP-treated
Spearman r= 0.7881 P<0.0001
nuclear dpERK signal
1500
1000
500
0
n=12 per cell type
0.0
0.1
0.2
0.3
0.4
relative contact area with A-line cells

Figure 2

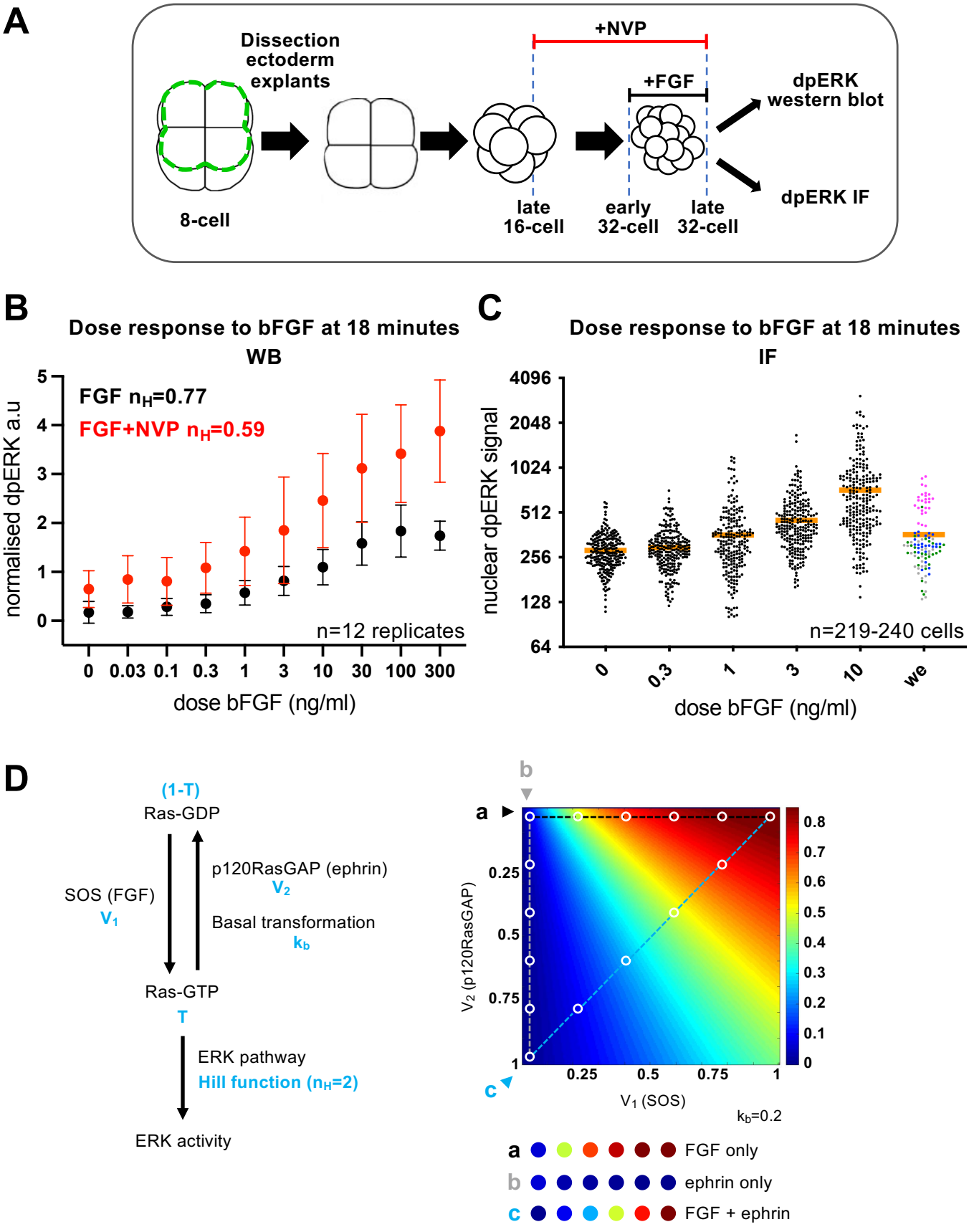
A
Dissection
ectoderm
explants
+NVP
+FGF
dpERK
western blot
dpERK IF
8-cell
late
16-cell
early
32-cell
late
32-cell
B
Dose response to bFGF at 18 minutes
WB
normalised dpERK a.u
FGF n_H=0.77
FGF+NVP n_H=0.59
n=12 replicates
dose bFGF (ng/ml)
C
Dose response to bFGF at 18 minutes
IF
nuclear dpERK signal
n=219-240 cells
dose bFGF (ng/ml)
D
(1-T)
Ras-GDP
SOS (FGF)
V_1
p120RasGAP (ephrin)
V_2
Basal transformation
k_b
Ras-GTP
T
ERK pathway
Hill function (n_H=2)
ERK activity
V_2 (p120RasGAP)
V_1 (SOS)
k_b=0.2
FGF only
ephrin only
FGF + ephrin

Figure 3

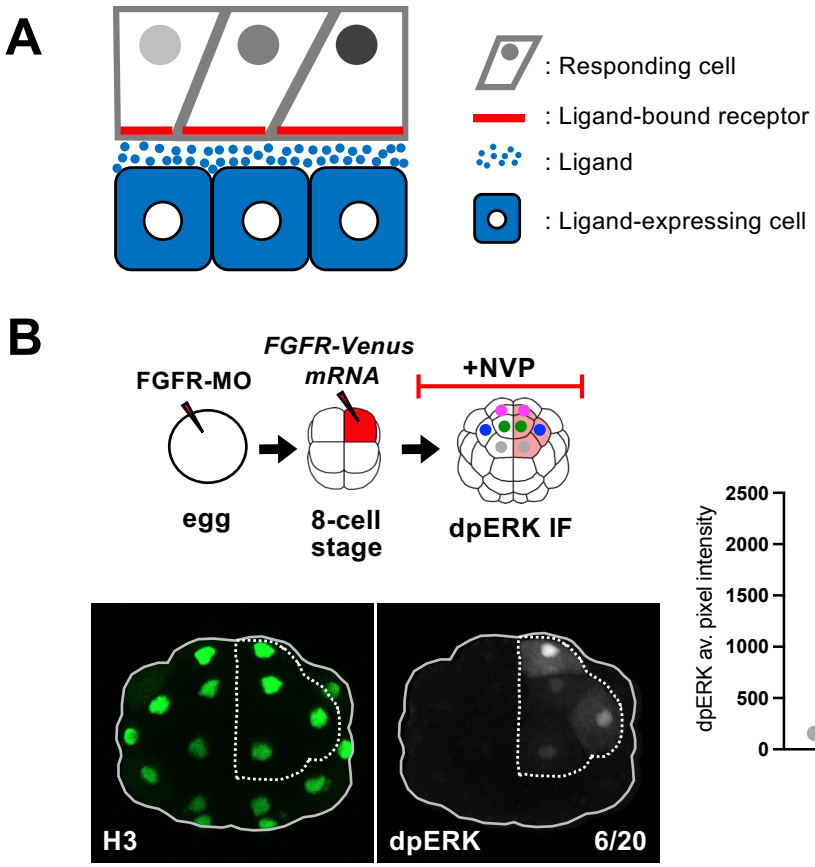
A
: Responding cell
: Ligand-bound receptor
: Ligand
: Ligand-expressing cell
B
FGFR-MO
FGFR-Venus mRNA
+NVP
egg
8-cell stage
dpERK IF
H3
dpERK
6/20
dpERK av. pixel intensity
100%
100%
95%
80%
70%
65%
****
****
****
**
ns
*
n=20
MO
MO +mRNA
C
ERK as function of R
Erk activity
n =2.6
Number of receptors in contact with FGF-expressing cells (a.u.)
ERK as function of [Fgf]
R =1000; nH =1.57
R =750 ; nH =1.44
R =500 ; nH =1.38
R =250 ; nH =1.21
FGF concentration (nM)
D
S1 to ERK
[Fgf] to ERK
Hill Coefficients
Ke
Kd
Krg
Ks
kb
K1
K2
Vrg
Vs

Figure 4

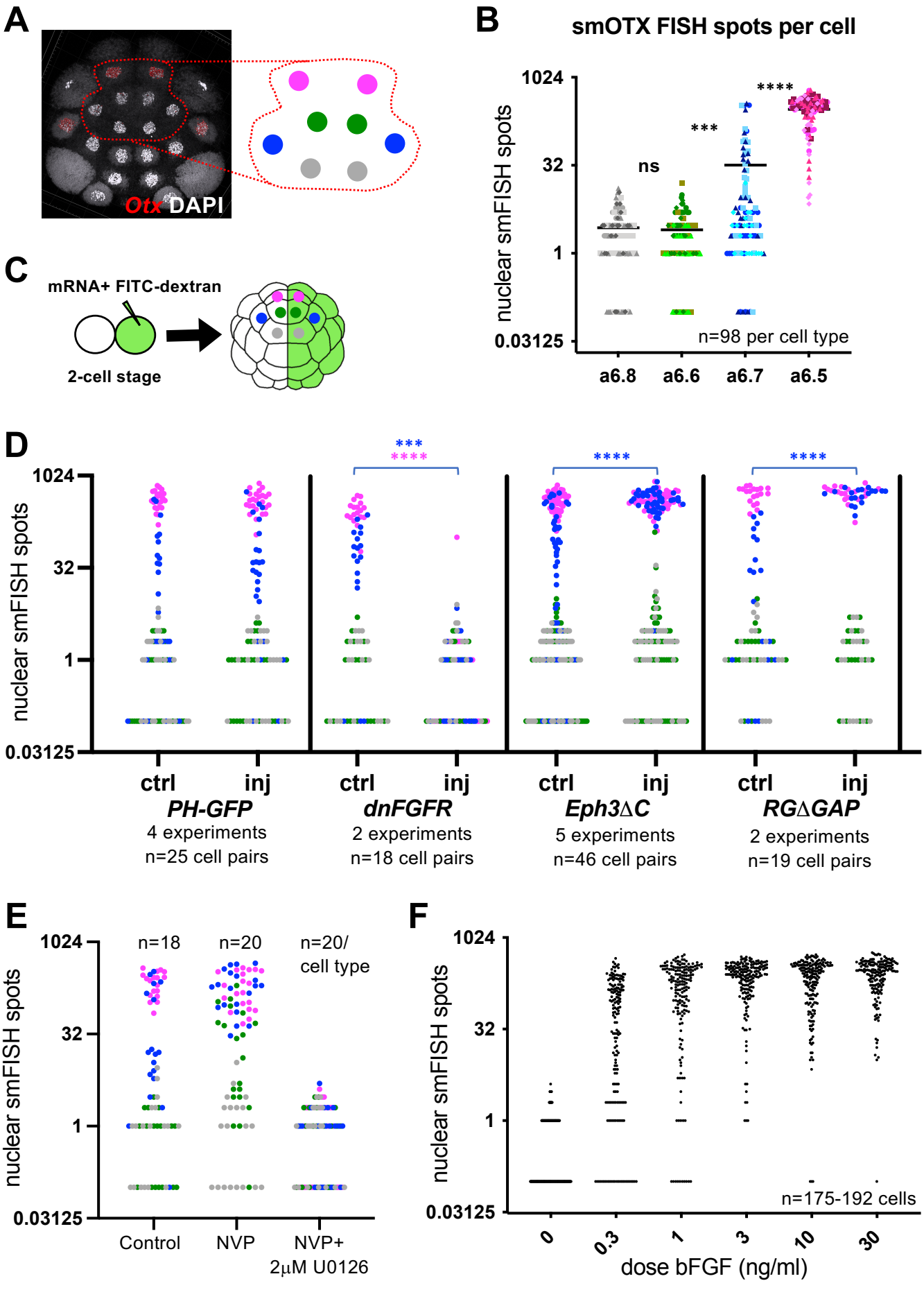
A
Otx DAPI
B
smOTX FISH spots per cell
nuclear smFISH spots
1024
32
1
0.03125
ns
***
****
n=98 per cell type
a6.8
a6.6
a6.7
a6.5
C
mRNA+ FITC-dextran
2-cell stage
D
nuclear smFISH spots
1024
32
1
0.03125
***
****
****
****
ctrl
inj
PH-GFP
4 experiments
n=25 cell pairs
dnFGFR
2 experiments
n=18 cell pairs
Eph3ΔC
5 experiments
n=46 cell pairs
RGΔGAP
2 experiments
n=19 cell pairs
E
nuclear smFISH spots
1024
32
1
0.03125
n=18
n=20
n=20/
cell type
Control
NVP
NVP+
2μM U0126
F
nuclear smFISH spots
1024
32
1
0.03125
n=175-192 cells
0
0.3
1
3
10
30
dose bFGF (ng/ml)

Figure 5

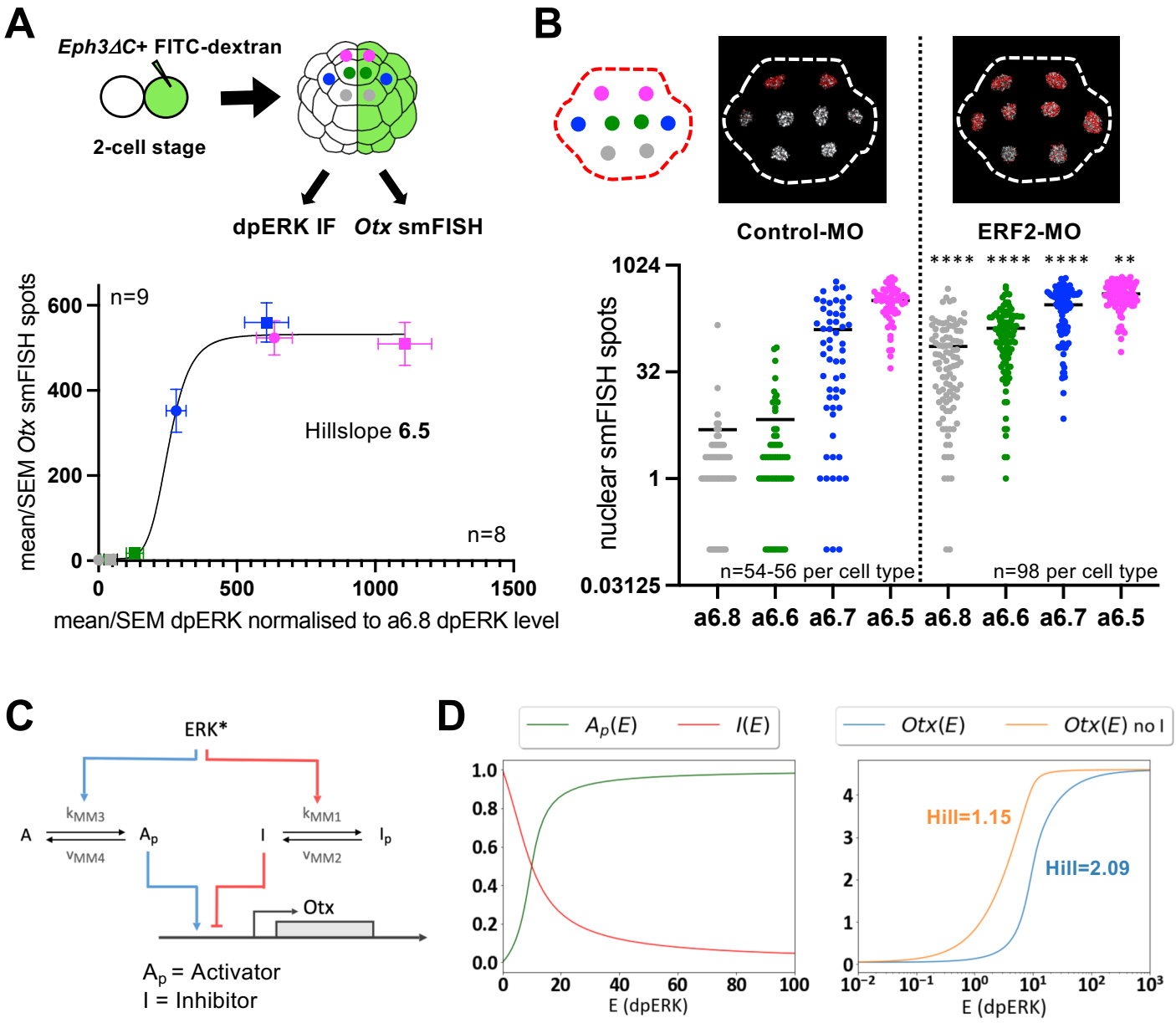
A
Eph3ΔC+ FITC-dextran
2-cell stage
dpERK IF
Otx smFISH
mean/SEM Otx smFISH spots
n=9
Hillslope 6.5
n=8
mean/SEM dpERK normalised to a6.8 dpERK level
B
Control-MO
ERF2-MO
nuclear smFISH spots
n=54-56 per cell type
n=98 per cell type
a6.8 a6.6 a6.7 a6.5 a6.8 a6.6 a6.7 a6.5
C
ERK*
Otx
Ap = Activator
I = Inhibitor
D
Ap(E)
I(E)
Otx(E)
Otx(E) no I
Hill=1.15
Hill=2.09
E (dpERK)

Figure 6

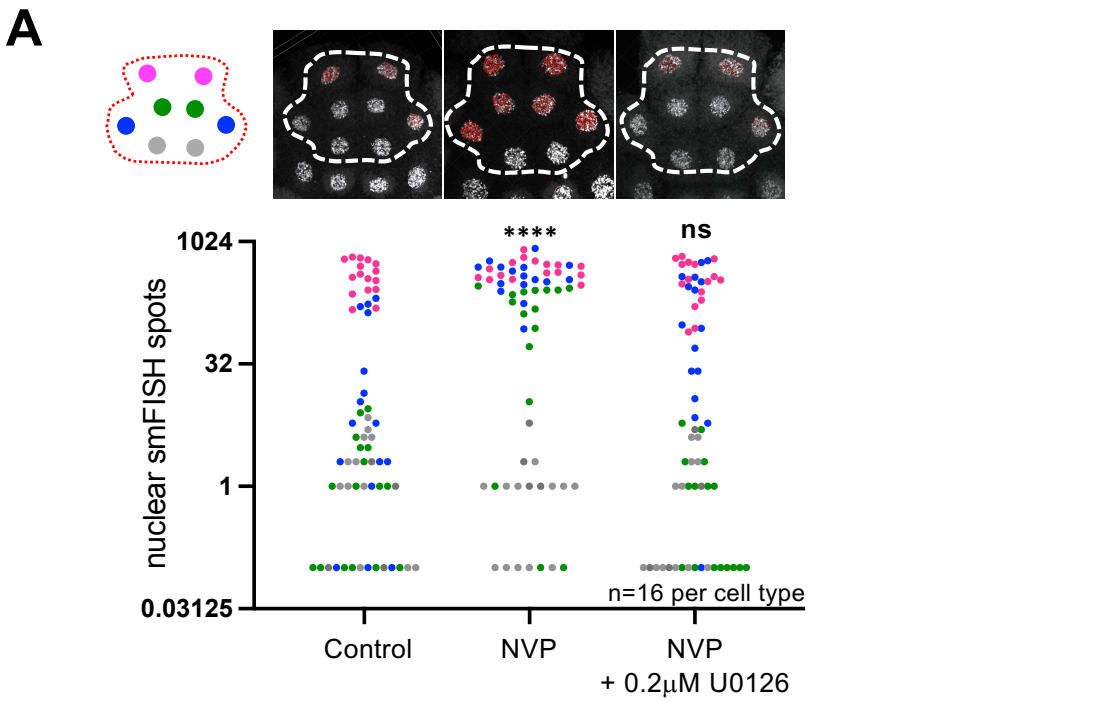
A
****
ns
1024
32
1
0.03125
nuclear smFISH spots
n=16 per cell type
Control
NVP
NVP
+ 0.2μM U0126

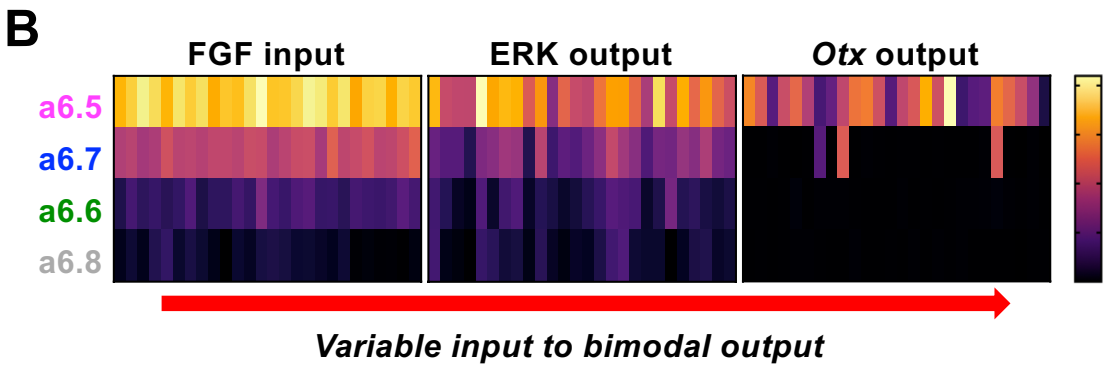
B
FGF input
ERK output
Otx output
a6.5
a6.7
a6.6
a6.8
Variable input to bimodal output

Figure 7

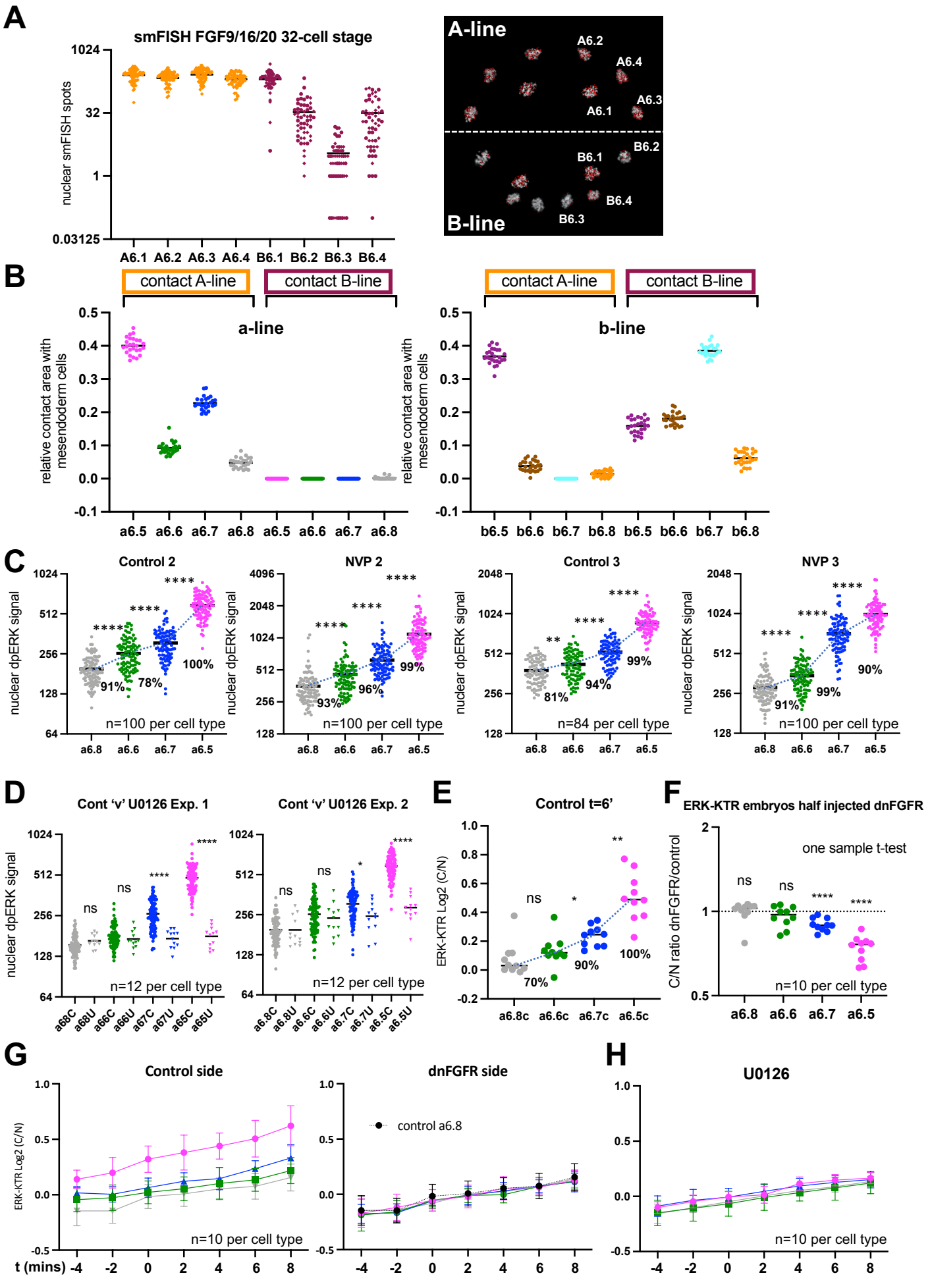
A
smFISH FGF9/16/20 32-cell stage
nuclear smFISH spots
1024
32
1
0.03125
A6.1 A6.2 A6.3 A6.4 B6.1 B6.2 B6.3 B6.4
A-line
A6.2
A6.4
A6.3
A6.1
B6.2
B6.1
B6.4
B6.3
B-line
B
contact A-line
contact B-line
a-line
b-line
relative contact area with mesendoderm cells
a6.5 a6.6 a6.7 a6.8 a6.5 a6.6 a6.7 a6.8
b6.5 b6.6 b6.7 b6.8 b6.5 b6.6 b6.7 b6.8
C
Control 2
NVP 2
Control 3
NVP 3
nuclear dpERK signal
91%
78%
100%
93%
96%
99%
81%
94%
99%
91%
99%
90%
n=100 per cell type
n=84 per cell type
D
Cont 'v' U0126 Exp. 1
Cont 'v' U0126 Exp. 2
nuclear dpERK signal
ns
n=12 per cell type
a6.8C a6.8U a6.6C a6.6U a6.7C a6.7U a6.5C a6.5U
E
Control t=6'
ERK-KTR Log2 (C/N)
70%
90%
100%
a6.8c a6.6c a6.7c a6.5c
F
ERK-KTR embryos half injected dnFGFR
one sample t-test
C/N ratio dnFGFR/control
n=10 per cell type
G
Control side
dnFGFR side
control a6.8
ERK-KTR Log2 (C/N)
n=10 per cell type
t (mins) -4 -2 0 2 4 6 8
H
U0126
n=10 per cell type

Figure S1

Figure S1. ERK activation in control, NVP- and U0126- treated embryos. Related to Figures 1 and 2. Data from different cell types are coloured as follows: a6.5 in magenta, a6.6 in green, a6.7 in blue and a6.8 in grey. A) Right: Imaris-segmented nuclear *FGF9/16/20* smFISH spots (red), counterstained with DAPI (white), of a 32-cell stage embryo in vegetal pole view. Cell names are indicated on the right-hand side of the embryo. Left: levels of *FGF9/16/20* transcripts are similar among A-line cells (orange), but different among the B-line cells (maroon). B) Relative area of surface contact with A-line and B-line mesendoderm cells (surface contact with mesendoderm/total cell surface) for each a-line ectoderm cell (left) and each b-line ectoderm cell (right). a-line ectoderm cells contact almost exclusively A-line mesendoderm cells, whereas b-line cells contact both A- and B-line cells. C) Mean pixel intensity of nuclear dpERK IF signal for each a-line cell for approximately 50 embryos processed under identical conditions (same tube, cover slip and acquisition session) for control untreated (Control) or NVP-treated (NVP) embryos. Control 2 and NVP 2 were obtained from the same batch of eggs and sperm, as were Control 3 and NVP 3. Control and NVP samples were processed on different days under different acquisition settings (see Figure S2C for 'same tube' comparisons between Control and NVP embryos). Statistical tests are two tailed paired t-tests comparing each cell-type based on the hierarchical order of their dpERK IF signal levels, i.e. comparing a6.5 to a6.7, a6.7 to a6.6, and a6.6 to a6.8. ** P<0.01; **** P<0.0001. D) Comparison of ERK activation levels in a-line cells between control untreated (C,●) and U0126-treated (U,▼) embryos processed in the same tube for anti-dpERK IF. Control untreated embryos in Exp. 1 and Exp. 2 correspond to those in Figure 1D and S1C, respectively. n= number of cells per cell type for U0126-treated embryos. Statistical tests are two tailed unpaired t-tests comparing each cell-type between control and U0126-treated embryos. ****P<0.0001, *P<0.05, ns P≥0.05. E-H) *Phallusia mammillata* embryos injected with *ERK-KTR-mClover* mRNA and *NLS-tdTomato* mRNA. Time-lapse movies were normalised to t=0 at the point of A6.4 nuclear envelope breakdown (NEBD). t= 4-8 corresponds to 'late 32-cell stage', when vegetal cells undergo de-compaction and embryos become flattened in shape. E, F and G use same data of embryos injected with *dnFGFR* mRNA in one cell at the 2-cell stage. E) ERK-KTR cytoplasmic/nuclear (C/N) ratio for each cell type at t=6' in control halves. Each dot on the graphs represents a single cell. Two-tailed paired t-tests compare a6.5 to a6.7, a6.7 to a6.6, and a6.6 to a6.8. **P<0.01, *P<0.05, ns P≥0.05. F) Graph shows injected/control ratios of ERK-KTR cytoplasmic/nuclear (C/N) ratios for each cell type in *dnFGFR* half-injected embryos at t=6'. n=number of ratios analysed for each cell-type; black bar = mean. Statistical tests are one sample two-tailed t-tests with a theoretical mean of 1. ****P<0.0001, ns P≥0.05. G) Mean + SD ERK-KTR C/N ratios for 32-cell stage a-line cells in control and *dnFGFR*-injected halves during the 32-cell stage. Control a6.8 trace (in black) groups with *dnFGFR* cells (right). H) Mean + SD ERK-KTR cytoplasmic/nuclear (C/N) ratio for a-line ectoderm cells during the 32-cell stage in U0126-treated embryos.

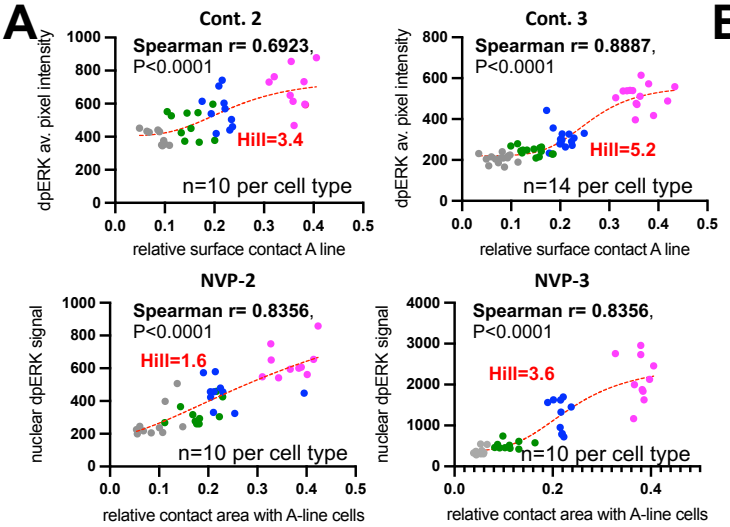

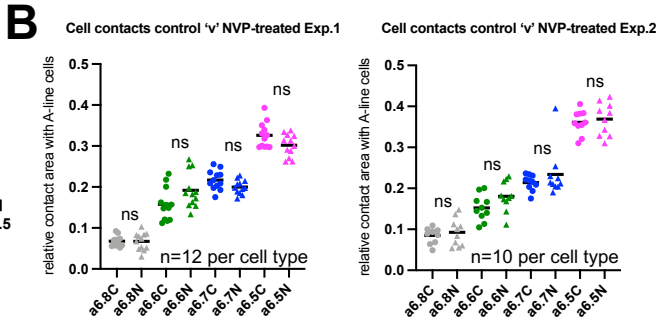

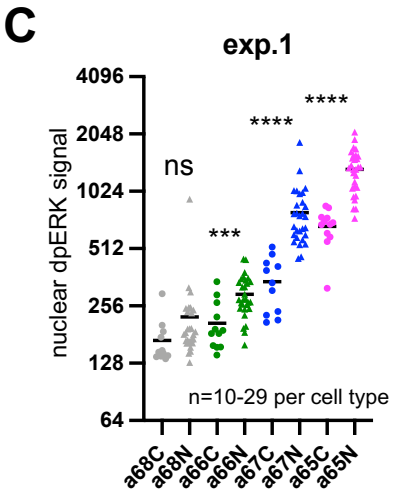

Experiment	Best fit Hill	CI Hill	R^2 Hill	spearman	CI spearman
NVP1 (48)	2,6	0,71 to 7,4	0,61	0,79 ****	0,64 to 0,88
NVP2 (40)	1,6	0,2 to ???	0,68	0,84 ****	0,70 to 0,91
NVP3 (40)	3,6	0,6 to 11	0,79	0,90 ****	0,81 to 0,95
NVP4 (24)	6,8	2,1 to 14,3	0,91	0,94 ****	0,86 to 0,98
NVP 5 (40)	9,5	3,3 to ???	0,78	0,85 ****	0,74 to 0,92
NVP 6 (80)	3,2	1,7 to 6,6	0,77	0,88 ****	0,82 to 0,92
NVP 7 (64)	5,8	3,3 to 9,7	0,90	0,91 ****	0,86 to 0,95
NVP 8 (56)	10,1	5,1 to 20	0,80	0,91 ****	0,84 to 0,95
Cont 1 (48)	3,9	??? to 11,4	0,54	0,76 ****	0,6 to 0,86
Cont 2 (40)	3,4	??? to 15	0,51	0,69 ****	0,48 to 0,83
Cont 3 (56)	5,2	2,5 to 10,7	0,86	0,89 ****	0,81 to 0,93
Cont 3ii (56)	3,6	1,1 to 12,1	0,80	0,88 ****	0,8 to 0,93

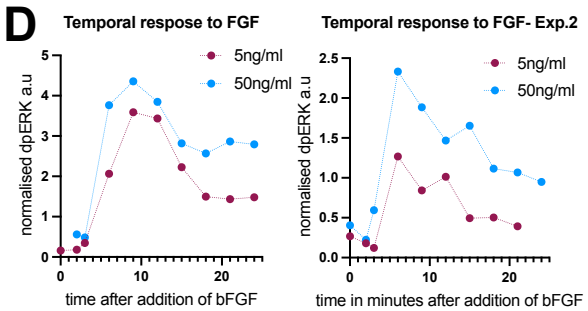

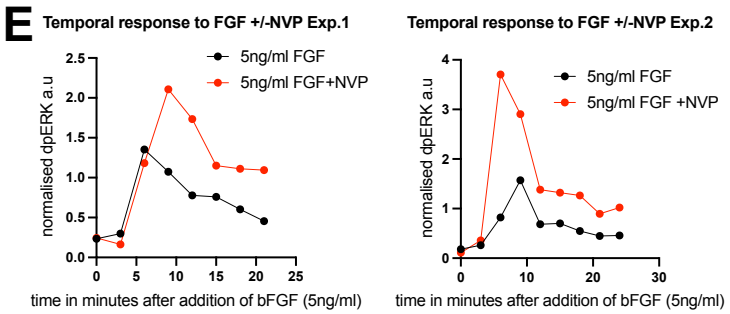

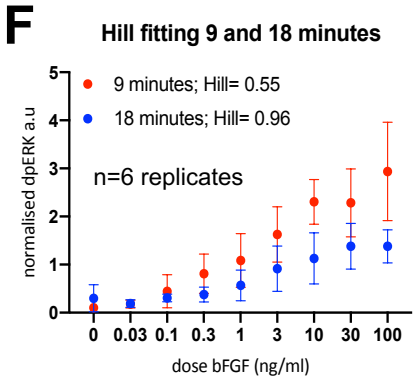

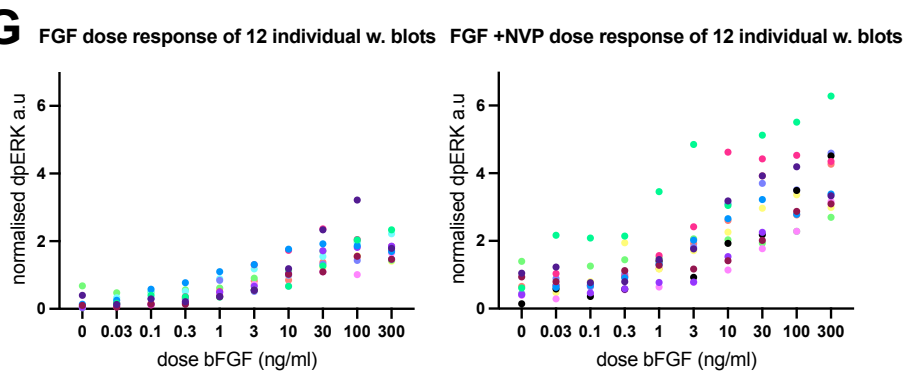

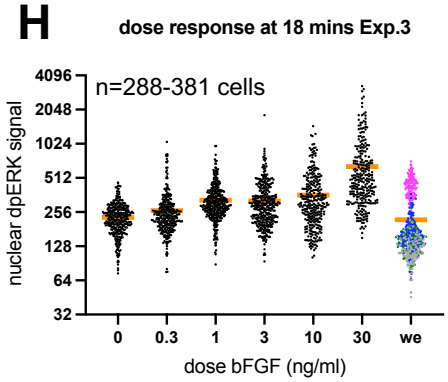

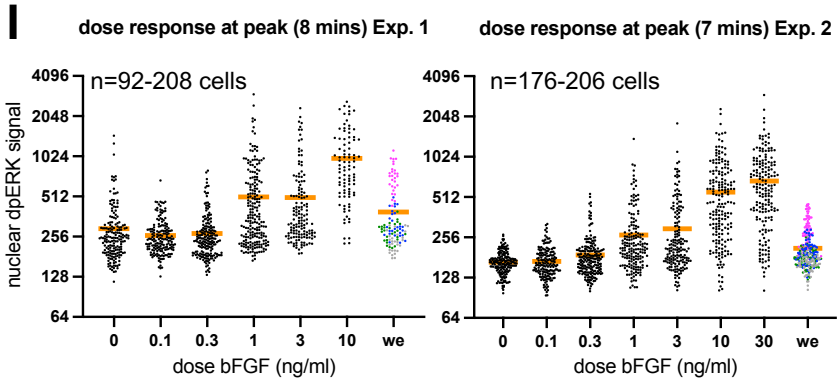

Figure S2

Figure S2. From FGF signal input to ERK activation in embryos and explants. Related to Figures 1-3. Data from different cell types are coloured as follows: a6.5 in magenta, a6.6 in green, a6.7 in blue and a6.8 in grey. A) Normalized ectoderm cell surface contact (contact surface/total surface) with A-line (mesendoderm) cells and mean pixel intensity of nuclear dpERK IF signal were obtained for each a-line ectoderm cell in control or NVP-treated embryos. Spearman correlations and best-fit Hill functions are shown on the graphs. The table shows these best-fit Hill coefficients and those obtained from additional experiments with the corresponding confidence intervals (CI Hill) and R^2 as well as the Spearman correlations and CI for Spearman correlations. 'Cont 3ii' represents a technical replicate of control 3 embryos, processed in a separate tube. In the table, the number in parenthesis represents the total number of cells analysed per experiment. B) Relative cell surface contact with A-line (mesendoderm) cells was obtained for each a-line ectoderm cell in control (C, ●) or NVP-treated (N, ▲) embryos. The data from experiment 1 is the same data as that in Figure 1E and 2D and experiment 2 is presented in A (Cont.2 and NVP-2). Statistical tests are two tailed unpaired t-tests comparing each cell-type in control versus NVP-treated embryos. ns, no significant difference ($P \geq 0.05$). C) Control embryos injected with fluorescent dextran were fixed in the same tube as embryos treated with 6-8μM NVP and processed under identical conditions. Treatment with 2μM, 4μM or 16μM NVP gave similar results, except 2μM appeared to have a slightly weaker effect (3 repetitions, not shown). Statistical tests are two tailed unpaired t-tests comparing each cell-type under control versus NVP-treated conditions from the same tube. ****$P<0.0001$, ***$P<0.001$, **$P<0.01$, ns $P \geq 0.05$. In five replicate experiments, significance tests for each cell type gave the following results: a6.5 control 'v' NVP- 5/5 ****; a6.7 control 'v' NVP- 5/5****; a6.6 control 'v' NVP- ****, ****, ***, ns, ns; a6.8 control 'v' NVP- ***, **, **, ns, ns. D-G) Western blot analyses of ERK activation in response to exogenous FGF. See STAR Methods for details of normalization procedure. D) Normalized α-dpERK western blot signal showing the temporal response of ERK activation in ectodermal explants treated with two doses of bFGF. E) Temporal responses to 5ng/ml bFGF in the presence or absence of NVP. In two additional independent experiments, embryos were treated with 50ng/ml bFGF with or without NVP and collected at 9 minutes for western blot analysis. In both cases, normalized dpERK levels were higher in the NVP-treated explants (not shown). For other doses at 18 minutes, see (G). F) Normalized α-dpERK western blot signal (mean ± SD) of 6 experimental replicates of dose response, with samples collected at 9 or 18 minutes after addition of bFGF. Curve fitting with Hill functions gave best-fit Hill coefficients (Hill=) as indicated. G) Individual western blot data from Figure 3B showing dpERK signal normalised to PKCζ and further normalised to whole embryo "standard" dpERK/PKCζ signal ratio in bFGF- (left) or bFGF- plus NVP- (right) treated explants (12 pairs of western blots). H-I) Each dot represents the mean pixel intensity of nuclear dpERK IF signal in single cell of ectoderm explants treated with different doses of bFGF. Untreated whole embryos were placed in the same tubes with explants (shown on the right of each graph; a6.5 in magenta, a6.6 in green, a6.7 in blue and a6.8 in grey). n=number of cells analysed in explants per dose of FGF. Mean indicated by orange bars. H) Samples were collected at 18 minutes following application of bFGF. I) Samples were collected during the 'peak' at 6-9 minutes, following application of bFGF.

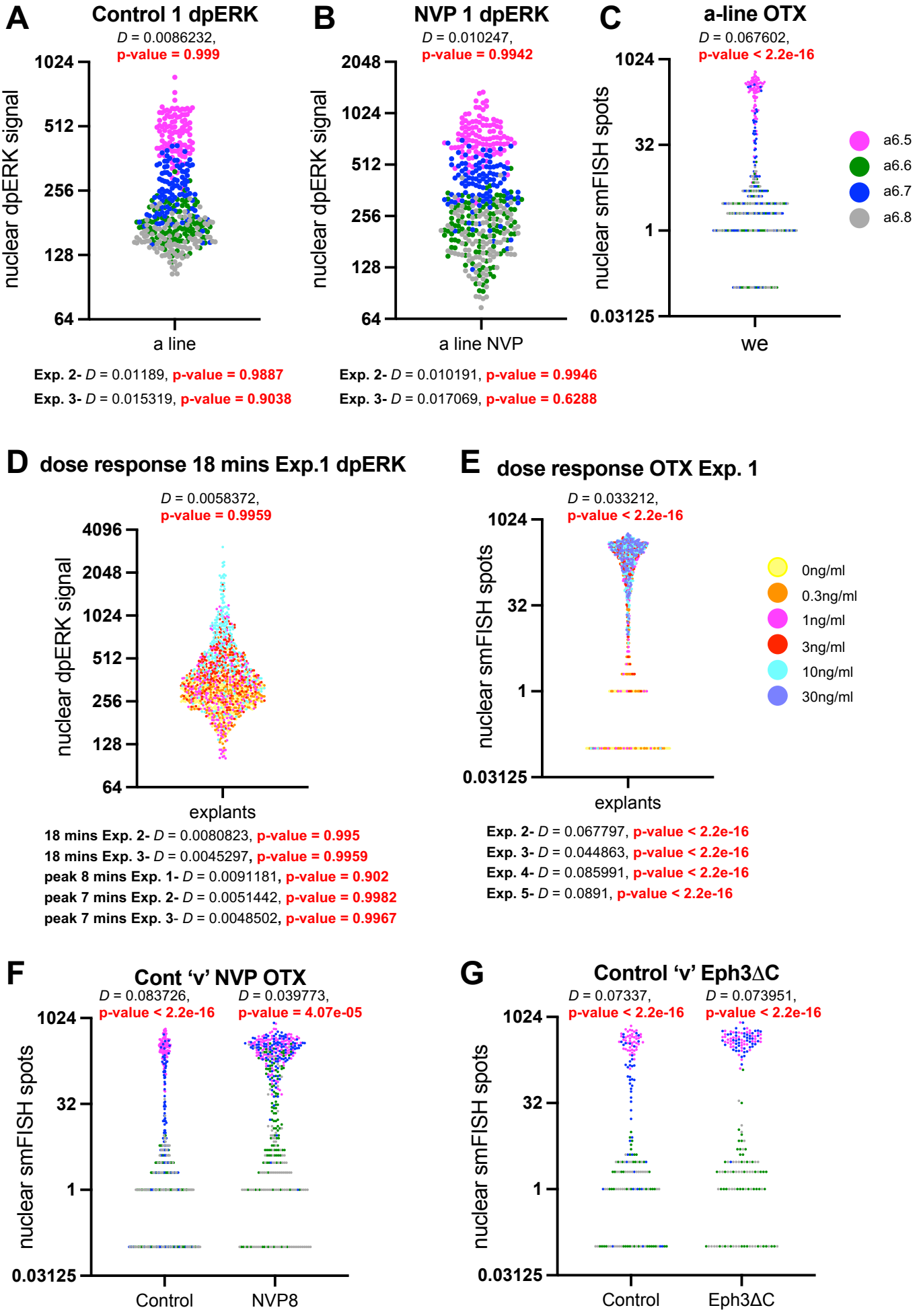
A
Control 1 dpERK
D = 0.0086232,
p-value = 0.999
nuclear dpERK signal
1024
512
256
128
64
a line
B
NVP 1 dpERK
D = 0.010247,
p-value = 0.9942
nuclear dpERK signal
2048
1024
512
256
128
64
a line NVP
C
a-line OTX
D = 0.067602,
p-value < 2.2e-16
nuclear smFISH spots
1024
32
1
0.03125
we
a6.5
a6.6
a6.7
a6.8
Exp. 2- D = 0.01189, p-value = 0.9887
Exp. 3- D = 0.015319, p-value = 0.9038
Exp. 2- D = 0.010191, p-value = 0.9946
Exp. 3- D = 0.017069, p-value = 0.6288
D dose response 18 mins Exp.1 dpERK
D = 0.0058372,
p-value = 0.9959
nuclear dpERK signal
4096
2048
1024
512
256
128
64
explants
18 mins Exp. 2- D = 0.0080823, p-value = 0.995
18 mins Exp. 3- D = 0.0045297, p-value = 0.9959
peak 8 mins Exp. 1- D = 0.0091181, p-value = 0.902
peak 7 mins Exp. 2- D = 0.0051442, p-value = 0.9982
peak 7 mins Exp. 3- D = 0.0048502, p-value = 0.9967
E dose response OTX Exp. 1
D = 0.033212,
p-value < 2.2e-16
nuclear smFISH spots
1024
32
1
0.03125
explants
0ng/ml
0.3ng/ml
1ng/ml
3ng/ml
10ng/ml
30ng/ml
Exp. 2- D = 0.067797, p-value < 2.2e-16
Exp. 3- D = 0.044863, p-value < 2.2e-16
Exp. 4- D = 0.085991, p-value < 2.2e-16
Exp. 5- D = 0.0891, p-value < 2.2e-16
F
Cont 'v' NVP OTX
D = 0.083726,
p-value < 2.2e-16
D = 0.039773,
p-value = 4.07e-05
nuclear smFISH spots
1024
32
1
0.03125
Control
NVP8
G
Control 'v' Eph3ΔC
D = 0.07337,
p-value < 2.2e-16
D = 0.073951,
p-value < 2.2e-16
nuclear smFISH spots
1024
32
1
0.03125
Control
Eph3ΔC

Figure S3

Figure S3. Unimodal ERK activation and bimodal *Otx* activation: Hartigan's diptest for unimodality. Related to Figures 1-3, 5, 7, S1, S2, and S6. For whole embryo analyses (A, B, C, F, G), dots representing different cell types are coloured as indicated in the key, top right. For explant analyses (D, E), dots representing single cells in explants treated with different doses of bFGF are coloured based on the dose of bFGF, following the key on the middle right. Hartigan's diptest results are indicated (*D*=) with the corresponding p-values in red. A) dpERK IF signal in control embryos from Figure 1D. The null hypothesis of a unimodal distribution is not rejected following Hartigan's diptest. Below the graph are the diptest results from additional independent experiments, Exp. 2 and Exp. 3 (Figure S1C). B) dpERK IF signal in NVP-treated embryos from Figure 2C. The null hypothesis of a unimodal distribution is not rejected following Hartigan's diptest. Below the graph are the diptest results from additional independent experiments, Exp. 2 and Exp. 3 (Figure S1C). C) *Otx* smFISH spot counts in control embryos, from Figure 5B. The null hypothesis of a unimodal distribution is rejected following Hartigan's diptest, suggesting at least a bimodal distribution. D) dpERK IF signal in explants treated with increasing doses of bFGF, from Figure 3C. The null hypothesis of a unimodal distribution is not rejected following Hartigan's diptest. Below the graph are the diptest results from additional independent experiments, 18 minutes Exp. 2 and 3 (Figure S2H and not shown); peak (7 or 8 minutes) Exp. 1-3 (Figure S2I and not shown). E) *Otx* smFISH spot counts in explants treated with increasing doses of bFGF, from Figure 5F. The null hypothesis of a unimodal distribution is rejected following Hartigan's diptest, suggesting at least a bimodal distribution. Below the graph are diptest results from additional independent experiments, Exp. 2-5 (Figure S6E and not shown). F) *Otx* smFISH spot counts in control and NVP- treated embryos pooled from Figures 5E, 7A, and S6A-D. The null hypothesis of a unimodal distribution is rejected following Hartigan's diptest, suggesting at least a bimodal distribution. G) *Otx* smFISH spot counts in control and *Eph3ΔC* mRNA injected embryo halves from Figure 5D. The null hypothesis of a unimodal distribution is rejected following Hartigan's diptest, suggesting at least a bimodal distribution.

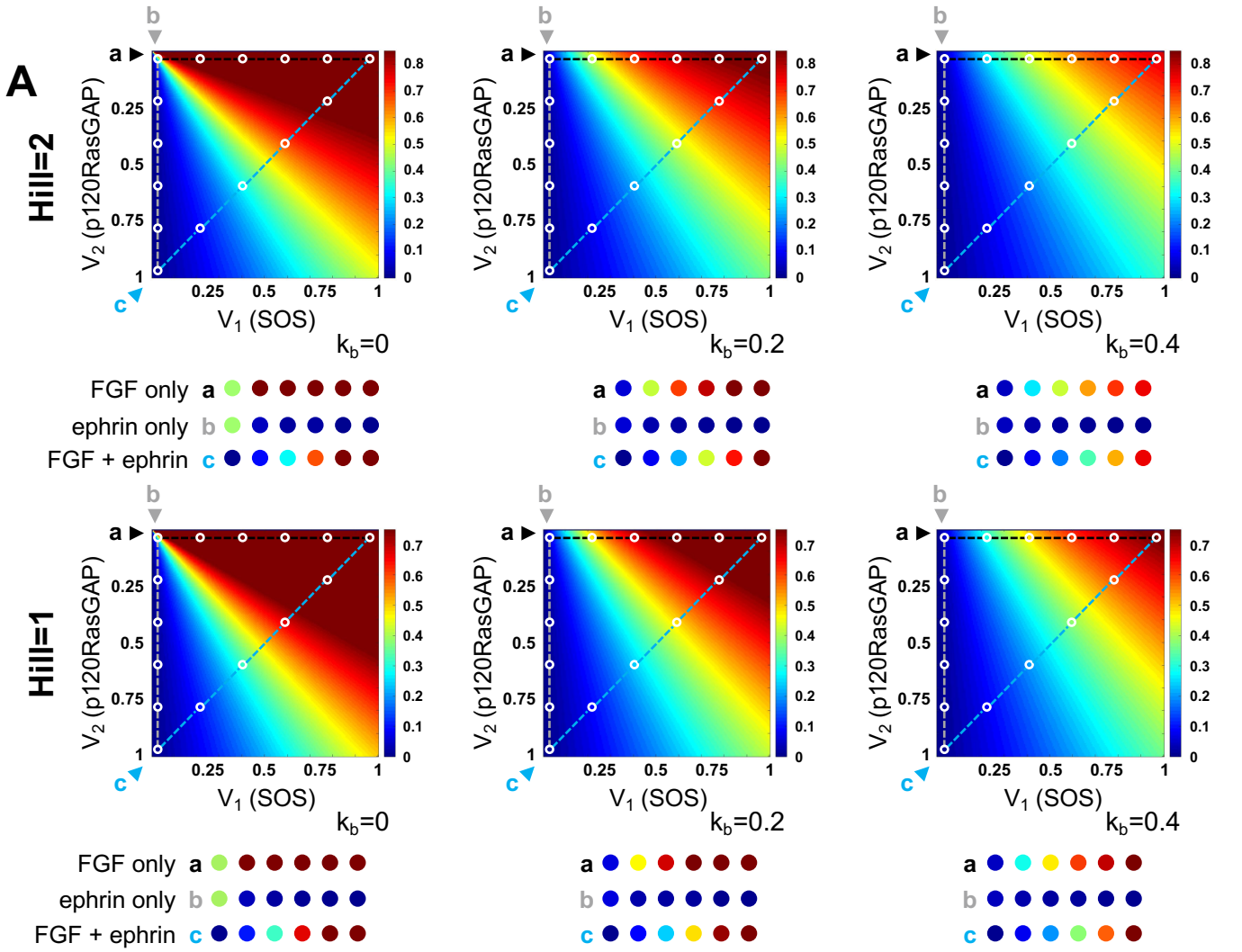
A
Hill=2
Hill=1
b
a
c
V2 (p120RasGAP)
V1 (SOS)
kb=0
kb=0.2
kb=0.4
FGF only a
ephrin only b
FGF + ephrin c

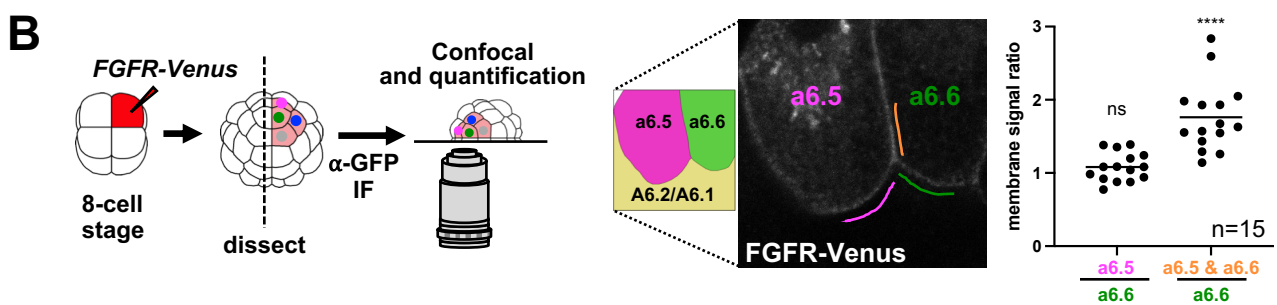
B
FGFR-Venus
8-cell stage
dissect
α-GFP IF
Confocal and quantification
a6.5
a6.6
A6.2/A6.1
FGFR-Venus
membrane signal ratio
ns
****
n=15
a6.5
a6.6
a6.5 & a6.6
a6.6

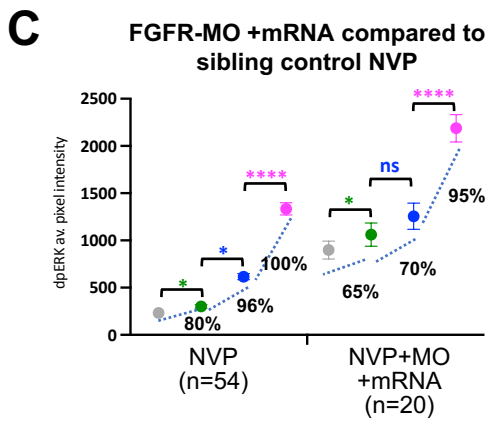
C
FGFR-MO +mRNA compared to sibling control NVP
dpERK av. pixel intensity
80%
96%
100%
65%
70%
95%
NVP (n=54)
NVP+MO +mRNA (n=20)

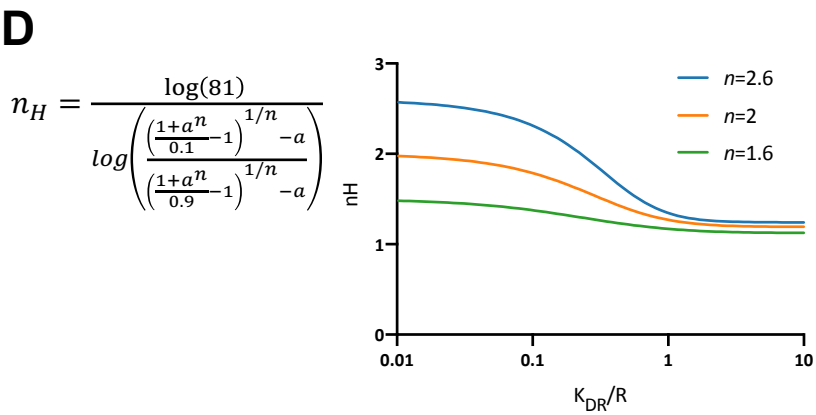
D
$n_H = \frac{\log(81)}{log\left(\frac{\left(\frac{1+a^n}{0.1}-1\right)^{1/n}-a}{\left(\frac{1+a^n}{0.9}-1\right)^{1/n}-a}\right)}$
nH
n=2.6
n=2
n=1.6
K_DR/R

Figure S4

Figure S4. From FGF signal input to ERK activation: modeling approach. Related to Figures 3 and 4. A) Graphical model outputs of ERK activation levels under control of SOS (V_1; FGF- signal input), p120RasGAP (V_2; ephrin- signal input) and basal GAPs (k_b), with p120RasGAP independent basal Ras GTPase-activating protein activity set at k_b =0, k_b =0.2 or k_b =0.4 and with Hill functions (Ras to ERK) set at 2 (above) or 1 (below). Below each heatmap graph are circles depicting six cells spread evenly across the differential inputs of FGF (SOS) and ephrin (p120RasGAP) signals at three different positions (colored arrowheads and white circles on the graph), **a**) differential SOS with no p120RasGAP (FGF only); **b**) differential p120RasGAP with no SOS (ephrin only); and **c**) both SOS and p120RasGAP (FGF + ephrin). The ERK heatmap with k_b =0 (left) is not consistent with experimental data as, in the absence of p120RasGAP activity, it predicts high ERK even at very low levels of SOS. B) Left: experimental procedure. We injected mRNA encoding *FGFR-Venus* into one a4.2 cell of the 8-cell stage, allowing us to measure mean α-GFP IF intensity at the interface between injected ectoderm and non-injected mesendoderm cells at the basal membrane of a6.5 and a6.6 at the mid 32-cell stage. Middle: maximum intensity z-projection of a confocal stack shows α-GPF IF staining in sagittal section of *FGFR-Venus* injected embryo. a6.5 and a6.6 basal membranes contact the mesendoderm cells, A6.2 and A6.1 (lower part of image), as shown on drawing. Mean pixel intensities were measured in the basal membrane of a6.5 (a6.5 basal) (above pink line) and a6.6 (a6.6 basal) (above green line) and in the lateral membrane between a6.5 and a6.6 (a6.5 & a6.6 lateral) (left of orange line). Right: membrane signal ratios (a6.5 basal/a6.6 basal and a6.5 & a6.6 lateral/a6.6 basal), each dot represents one embryo ratio; bar=mean. The α-GFP IF signal intensity ratios between a6.5 and a6.6 show no statistically significant difference from 1. On the other hand, the signal intensity ratios comparing the lateral membrane between a6.5 and a6.6 and the basal membrane of a6.6 showed a statistically significant increase from 1, which is expected since the lateral measurement includes labelled membranes of both a6.5 and a6.6. Statistical tests are one sample two-tailed t-tests with a theoretical mean of 1. ****P<0.0001, ns P≥0.05. C) Mean plus SEM of the mean pixel intensity of nuclear dpERK IF signal for each cell type of NVP-treated sibling embryos treated in the same dish/tube/coverslip/acquisition session as FGFR-MO+*FGFR-Venus* mRNA (a4.2) embryos from Figure 4B. Two-tailed paired t-tests per embryo half compare a6.5 to a6.7, a6.7 to a6.6 and a6.6 to a6.8, **** P<0.0001, * P<0.05, ns P≥0.05. Percentages represent the number of half embryos in which a6.5>a6.7, a6.7>a6.6 and a6.6>a6.8. n= number of cells analysed per cell type. D) The analytical expression given by equation (11) describes the relationship between the Hill coefficient with respect to FGF concentration, n_H, and the Hill coefficient with respect to the number of receptors exposed to FGF, n. The graph of n_H in relation to n shows that, whatever the value of n, n_H can only be smaller to or equal to n. The exact n depends on a, which is the ratio of the K_{DR} (the number of ligand-bound R at half maximum ERK activity) to R (the number of receptors exposed to ligand). The larger the K_{DR}/R, the lower the n_H.

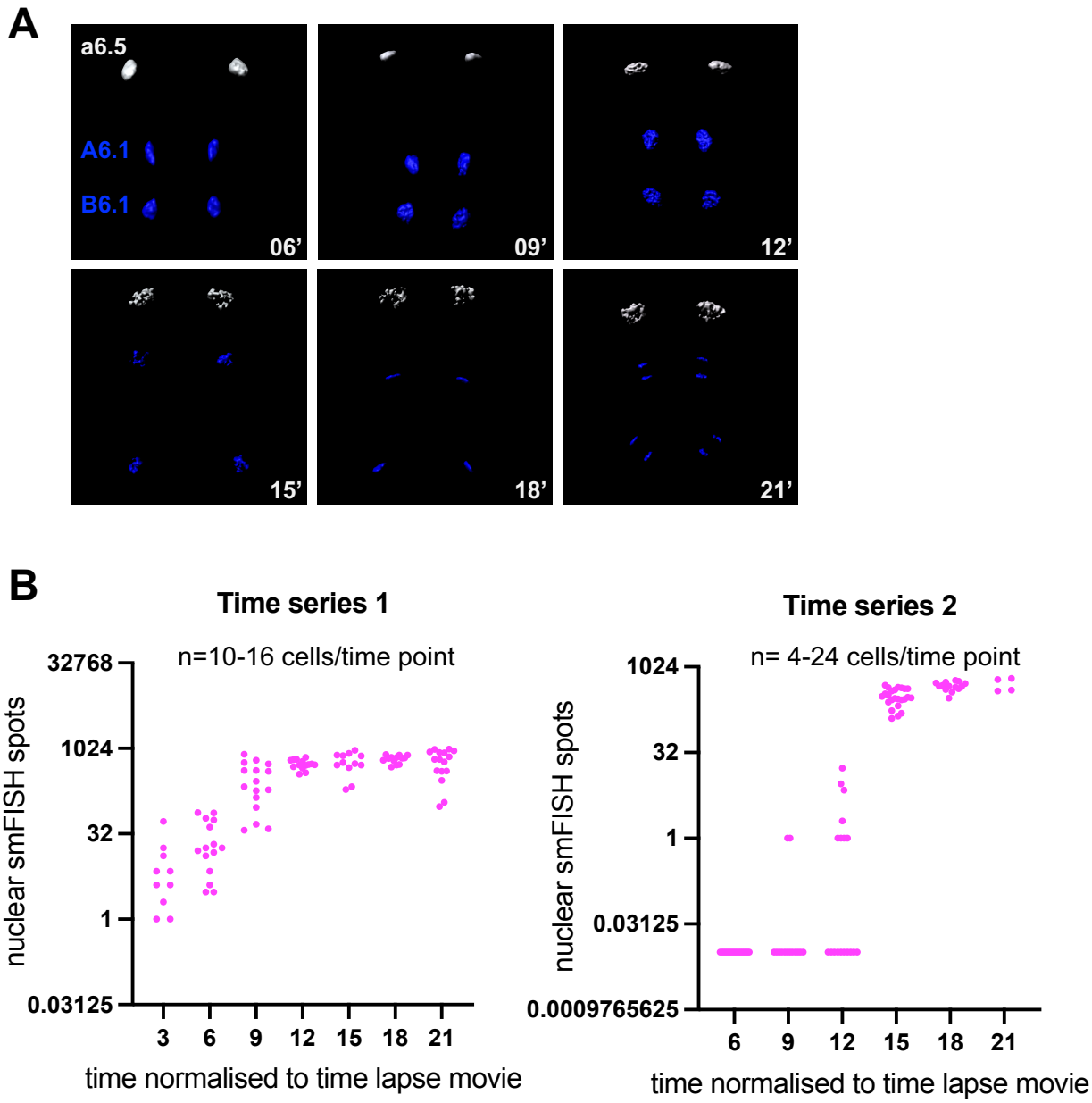
A
a6.5
A6.1
B6.1
06'
09'
12'
15'
18'
21'
B
Time series 1
n=10-16 cells/time point
nuclear smFISH spots
32768
1024
32
1
0.03125
3
6
9
12
15
18
21
time normalised to time lapse movie
Time series 2
n= 4-24 cells/time point
nuclear smFISH spots
1024
32
1
0.03125
0.0009765625
6
9
12
15
18
21
time normalised to time lapse movie
C
a6.5 Time series 2
06'
09'
12'
15'
18'
21'

Figure S5

Figure S5. Temporal profile of *Otx* transcriptional activation in a6.5. Related to Figure 5. For this experiment, synchronised batches of embryos were chosen, collected every 3 minutes and processed for *Otx* smFISH. To ensure correct time categories, snapshots of endoderm cell nuclei were taken and matched to a time-lapse movie of endoderm cells so that each individual embryo was time adjusted to match this movie (see STAR Methods for details). A) Composite confocal images highlight nuclei of endoderm cells (A6.1 and B6.1, blue) and a6.5 cells (white), showing the relative positions and shape of the endoderm and a6.5 nuclei in different categories of time: 3-6 minutes (06'), 6-9 minutes (09') etc. B) In two independent experiments, embryos were fixed every 3 minutes and adjusted for developmental time based on the position and morphology of endoderm and a6.5 cell nuclei (A). The graphs show the number of *Otx* smFISH spots counted in a6.5 nuclei at each developmental time. Every dot represents a single a6.5 cell. C) Snapshots of Imaris 3D visualisations of confocal stacks of a6.5 cell pairs, showing *Otx* smFISH spots (red) and DAPI (blue) at adjusted time points, from Time Series 2, prior to nuclear segmentation.

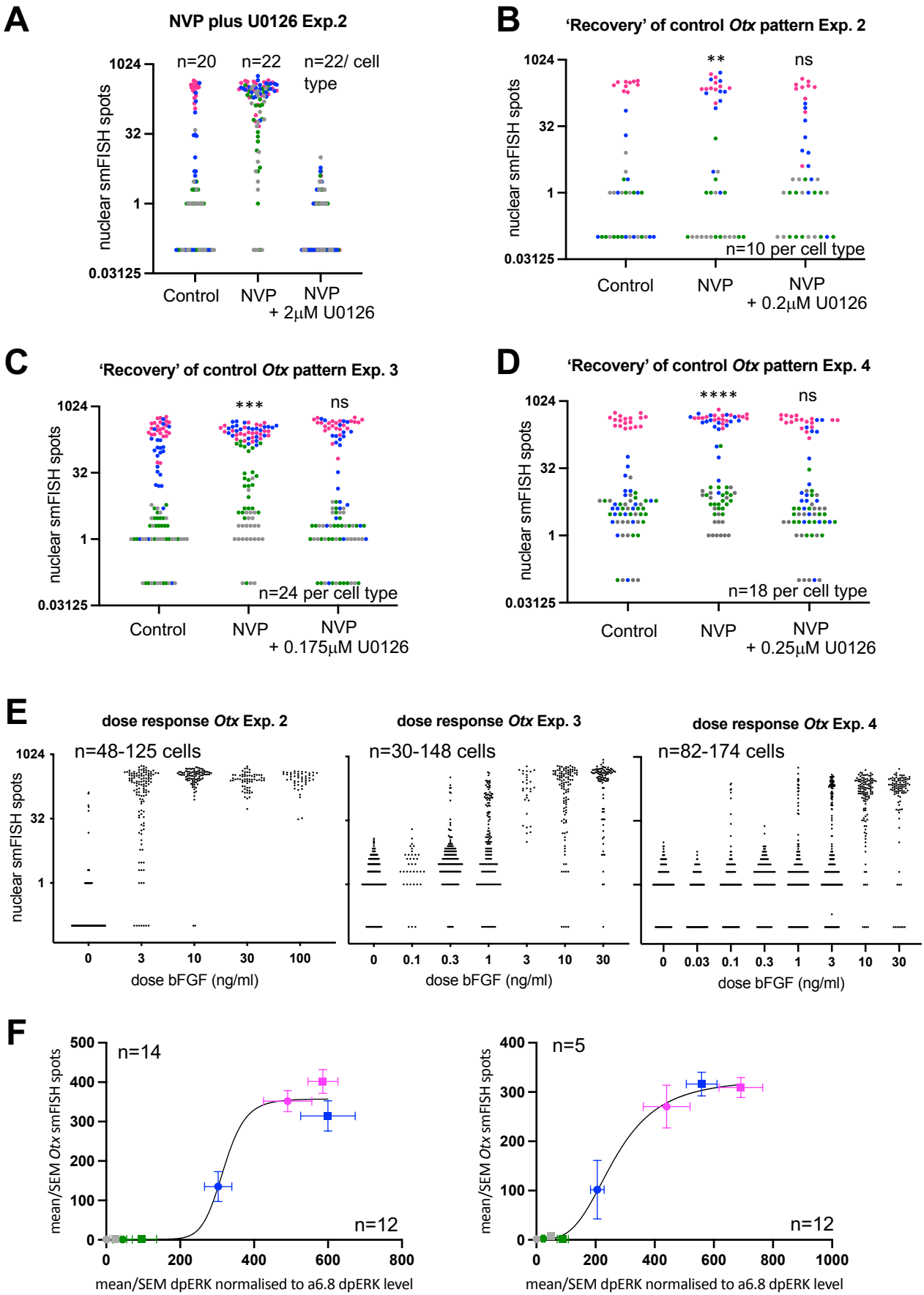
A
NVP plus U0126 Exp.2
n=20
n=22
n=22/ cell type
nuclear smFISH spots
1024
32
1
0.03125
Control
NVP
NVP + 2μM U0126
B
'Recovery' of control Otx pattern Exp. 2
**
ns
n=10 per cell type
Control
NVP
NVP + 0.2μM U0126
C
'Recovery' of control Otx pattern Exp. 3
***
ns
n=24 per cell type
Control
NVP
NVP + 0.175μM U0126
D
'Recovery' of control Otx pattern Exp. 4
****
ns
n=18 per cell type
Control
NVP
NVP + 0.25μM U0126
E
dose response Otx Exp. 2
n=48-125 cells
dose response Otx Exp. 3
n=30-148 cells
dose response Otx Exp. 4
n=82-174 cells
dose bFGF (ng/ml)
F
n=14
n=12
mean/SEM Otx smFISH spots
mean/SEM dpERK normalised to a6.8 dpERK level
n=5
n=12

Figure S6

Figure S6. Quantitative analyses of *Otx* expression. Related to Figure 5-7.
A-D) The graphs show the number of *Otx* smFISH spots per nucleus in each a-line cell following the treatments indicated. Data from different cell types are coloured as follows: a6.5 in magenta, a6.6 in green, a6.7 in blue and a6.8 in grey. A) Inhibition of Eph signaling (NVP) results in ectopic activation of *Otx*. Addition of high doses of U0126 (2μM) to NVP-treated embryos supresses activation of *Otx*. B-D) Inhibition of Eph signaling (NVP) results in ectopic activation of *Otx* in a6.7 and a6.6. Addition of low doses of U0126 (indicated on the graph) to NVP-treated embryos recovers the control expression pattern of *Otx*. For statistical tests, *Otx* smFISH spot counts were re-tabulated based on treatment and cell type and a 2-way ANOVA analysis was conducted comparing control to each experimental condition. The results of the 2-way ANOVA analyses are placed above each experimental condition: ** $P<0.01$; *** $P<0.001$; **** $P<0.0001$; ns $P\geq 0.05$. E) Each dot represents *Otx* smFISH spots per nucleus in individual cells of ectoderm explants treated with increasing doses of bFGF. n= the range of number of cells analysed for each dose. F) Following the procedure in Figure 6A, mean pixel intensity of nuclear dpERK IF signal and *Otx* smFISH spot count for each cell type in groups of control (●) and *Eph3ΔC*-injected (■) half embryos were obtained; mean dpERK IF signal was normalized by subtracting mean control side a6.8 signal (a6.8 = 0). Graphs show mean and SEM of these measurements for each cell type. Non-linear regression gave a best-fit Hill coefficient of 10.7 (left) and 3.4 (right). 95% confidence intervals (CI) are 1.0 to ? (upper limit could not be calculated) and 2.2 to 6.5, respectively. R^2 is 0.983 and 0.998, respectively.

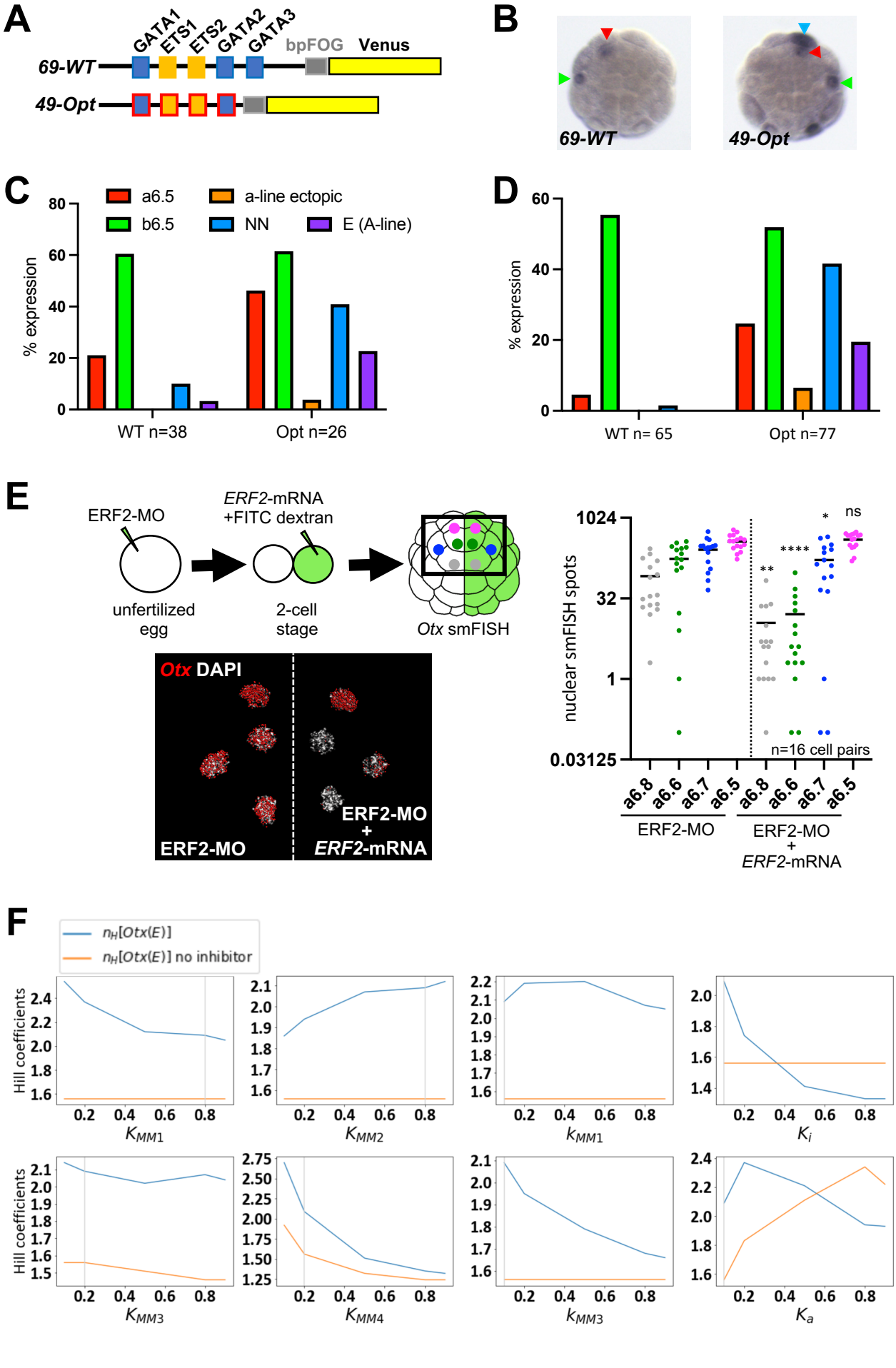
A
GATA1
ETS1
ETS2
GATA2
GATA3
bpFOG
Venus
69-WT
49-Opt
B
69-WT
49-Opt
C
a6.5
a-line ectopic
b6.5
NN
E (A-line)
% expression
WT n=38
Opt n=26
D
% expression
WT n= 65
Opt n=77
E
ERF2-MO
ERF2-mRNA
+FITC dextran
unfertilized
egg
2-cell
stage
Otx smFISH
Otx DAPI
ERF2-MO
ERF2-MO
+
ERF2-mRNA
nuclear smFISH spots
n=16 cell pairs
ERF2-MO
ERF2-MO
+
ERF2-mRNA
F
nH[Otx(E)]
nH[Otx(E)] no inhibitor
Hill coefficients
KMM1
KMM2
kMM1
Ki
KMM3
KMM4
kMM3
Ka

Figure S7

Figure S7. An inhibitor contributes to the spatial precision of *Otx* expression. Related to Figure 6. A-D) To address whether sub-optimization might contribute to the spatial precision of *Otx* gene expression among ectoderm cells at the 32-cell stage, we electroporated embryos with either the wild-type *Otx* a-enhancer (*Otx 69-WT*) or an optimized version, *Otx-49-Opt* (A) (Farley et al, 2015), detecting reporter gene (*Venus*) activation by ISH at the 32-cell stage (B). Expression was counted in a6.5, b6.5, ectopic a-line (a6.6, a6.7 and a6.8) and the A-line mesendoderm cells corresponding to NN (notochord-neural) and E (endoderm) cells. While we readily detected an increase in transgene activation in A-line cells (blue and purple bars), where ERK is also active, we detected ectopic transgene activation in a-line cells only very rarely and this ectopic activation was always restricted to a6.7 (orange bars) (C, D). This suggests that sub-optimization of the a-enhancer does not play a major role in the spatial precision of *Otx* gene activation in ectoderm cells at the 32-cell stage. A) Drawings of the transgenes used, red boxes indicate optimized sites (Farley et al, 2015). B) Example of reporter gene expression, showing *69-WT* activity (left) in a6.5 and b6.5 and *49-Opt* activity (right) in a6.5 and b6.5 and NN cells. C, D) Two independent experimental results showing percentage of embryos in which reporter gene activation was detected in at least one cell of the categories indicated. E) Top: experimental procedure. ERF2-MO was injected into unfertilized eggs. *ERF2*-mRNA was injected in one cell of the 2-cell stage embryo. Injection of mRNA resulted in a strong reduction in the ectopic expression of *Otx* resulting from *ERF2* knockdown. Image shows Imaris segmented nuclear smFISH *Otx* spots (red) in a-line cells from ERF2-MO and ERF2-MO plus *ERF2* mRNA sides, DAPI counterstain in white. Graph shows quantification of ERF2-MO rescue. Each spot represents a single cell, bar=mean. F) Comparison between the Hill coefficient of *Otx*(E) in the absence (orange lines) or presence (blue lines) of the inhibitor. Standard parameter set used in Figure 6D are indicated by vertical grey lines (see also STAR Methods for details). Varying the parameters in equations (21), (22) and (23) (see STAR Methods), we found that for a wide range of parameter values, the Hill obtained in the presence of the inhibitor is higher than in the absence of inhibitor.